

Potent and Subtype-Selective Dopamine D₂ Receptor Biased Partial Agonists Discovered via an Ugi-Based Approach

Ana Mallo-Abreu, Irene Reyes-Resina, Jhonny Azuaje, Rafael Franco, Aitor García-Rey, Maria Majellaro, Darío Miranda-Pastoriza, Xerardo García-Mera, Willem Jespers, Hugo Gutiérrez-de-Terán, Gemma Navarro,* and Eddy Sotelo*

Cite This: *J. Med. Chem.* 2021, 64, 8710–8726

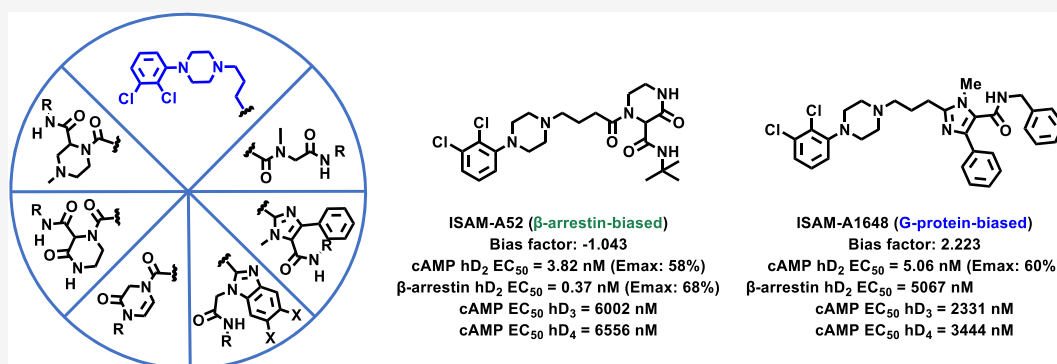
Read Online

ACCESS |

Metrics & More

Article Recommendations

Supporting Information



ABSTRACT: Using a previously unexplored, efficient, and versatile multicomponent method, we herein report the rapid generation of novel potent and subtype-selective DRD₂ biased partial agonists. This strategy exemplifies the search for diverse and previously unexplored moieties for the secondary/allosteric pharmacophore of the common phenyl-piperazine scaffold. The pharmacological characterization of the new compound series led to the identification of several ligands with excellent DRD₂ affinity and subtype selectivity and remarkable functional selectivity for either the cAMP (22a and 24d) or the β -arrestin (27a and 29c) signaling pathways. These results were further interpreted on the basis of molecular models of these ligands in complex with the recent DRD₂ crystal structures, highlighting the critical role of the secondary/allosteric pharmacophore in modulating the functional selectivity profile.

INTRODUCTION

The superfamily of seven transmembrane receptors (7TMR), commonly referred to as G protein-coupled receptors (GPCRs), is the largest target class in the druggable genome.¹ The receptors in this superfamily regulate virtually every aspect of human physiology, and they are sensors of a wide array of extracellular stimuli.¹ As a consequence, GPCRs are the target of more than 30% of all prescription drugs.² The synergistic use of innovative experimental and computational approaches in the last decade led to the increasing appreciation of the key role of conformational plasticity on GPCR signaling events (e.g., constitutive activity, inverse agonism, or biased agonism).³ For a number of GPCRs, the propensity to activate distinct G proteins can elicit diverse responses depending on the cellular environment.⁴ However, an even more subtle but intriguing mode of signaling has been attributed to the ability of a receptor to activate signaling pathways independent of G-protein activation. This occurs through the scaffolding of signaling complexes by β -arrestin, a component of the GPCR desensitization and internalization machinery.^{5,6} The process

by which ligands differentially modulate G-protein-dependent and/or G-protein-independent (β -arrestin) pathways to mediate specific downstream signal transduction routes is a phenomenon known as functional selectivity or biased agonism.³

The concept of biased agonism has progressively reshaped our understanding of GPCR signaling and shifted the paradigm of GPCR drug discovery.^{7,8} However, the molecular mechanisms behind biased signaling remain elusive since the study of the functional contributions of G-protein and β -arrestin mediated signaling pathways of endogenous/exogenous ligands still constitute a challenge.^{7,9} Biased GPCR ligands can trigger a specific pathway that is responsible for a

Received: April 19, 2021

Published: June 10, 2021



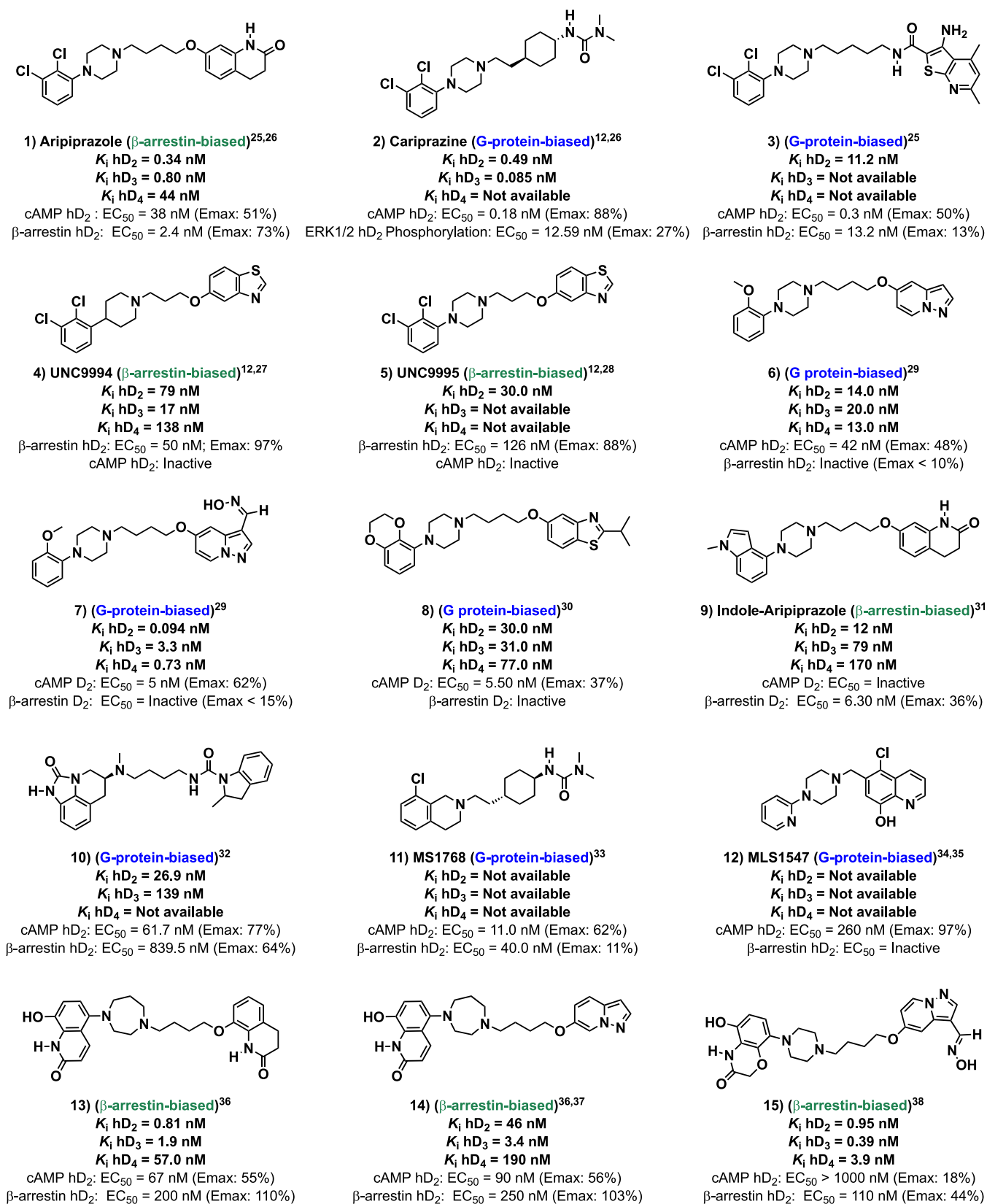


Figure 1. Selected examples from the literature of DRD₂ biased ligands.^{12,25–38}

given therapeutic effect, while not activating other signaling events eventually implicated in side effects. Such ligands are extremely useful to elucidate the key structural contributors to signal transduction pathways, besides their significant potential

to develop therapeutic agents with fewer side effects.^{10–12} A paradigmatic case is Oliceridine, a G-protein-biased μ -opioid (MOR) agonist that has shown encouraging results in clinical studies, combining a potent analgesic effect with reduced

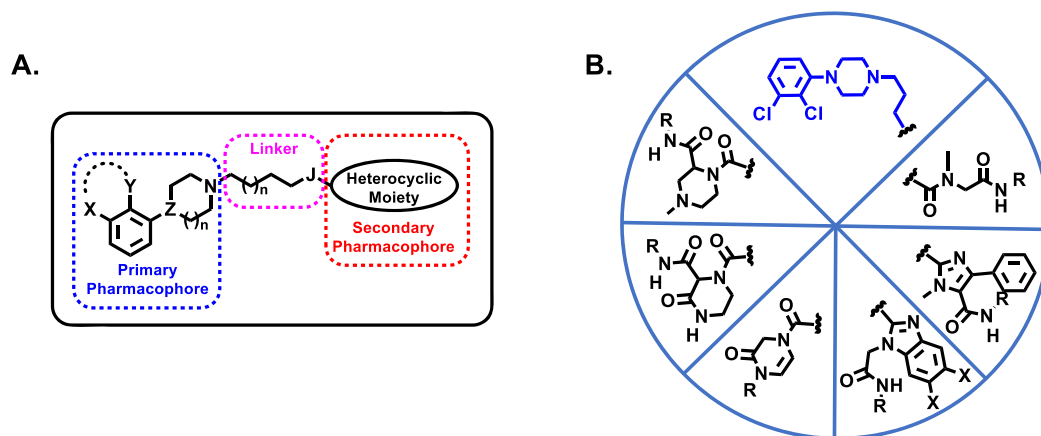


Figure 2. (A) Representative structure of most DRD₂ biased ligands. (B) General structure of herein described ligands. Blue: common (primary) pharmacophore in the series. Black: structure of the scaffolds explored in the secondary pharmacophore.

incidence of β -arrestin-mediated adverse effects (e.g., respiratory depression and constipation).^{13–15}

The dopamine D₂ receptor (DRD₂) is a prototypical GPCR for which exploration of the biased agonism concept is becoming the new paradigm to provide better drugs.^{12,16,17} DRD₂ is the primary target of antipsychotics and antiparkinsonian agents and is also implicated in the mode of action of several drugs associated with abuse and addiction.^{18,19} Schizophrenia is characterized by positive, negative, and cognitive symptoms.²⁰ Classical antipsychotics are effective at targeting the positive symptoms, but they do have adverse extrapyramidal symptoms (EPS).²¹ Atypical antipsychotics have overcome some of the problems associated with typical APDs in the clinic, and they are better at targeting the positive symptoms of schizophrenia without inducing EPS. However, these compounds have their own distinct side-effect profile, which includes weight gain, agranulocytosis, and hypotension.²¹ Aripiprazole and cariprazine (Figure 1) are prototypes of a new generation of atypical antipsychotics,²² and they were approved by the FDA for the treatment of schizophrenia, bipolar I manic/mixed episodes, and depressive disorder.²³ From a structural point of view, they are considered bitopic ligands, bearing a canonical primary pharmacophore (arylpiperazine) and a secondary (or allosteric) pharmacophore linked through an spacer group²⁴ (Figure 1). These drugs changed the view of antipsychotic action on dopamine signaling and introduced for the first time in the treatment of psychosis a clinically relevant mechanism based on DRD₂ occupancy without DRD₂ blockade. They are thought to act as antagonists in the striatum, where excessive dopamine activity is believed to cause positive symptoms, but they do show agonist activity in the mesocortical pathway, where reduced dopamine activity is associated with negative symptoms and cognitive impairment.²⁵

Inspired by the unique antipsychotic profile of aripiprazole, a novel series of DRD₂ biased agonists have been developed over the past decade (Figure 1). Inspection of the pharmacological data available for these ligands enabled to identify DRD₂ partial agonists eliciting either β -arrestin mediated recruitment and G-protein biased DRD₂ ligands (Figure 1). A structural analysis reveals their chemical analogy, particularly with the atypical antipsychotics that inspired their design (Figure 1). While effective in retaining the desired biased profiles, the limited structural diversity inherent to their design hindered

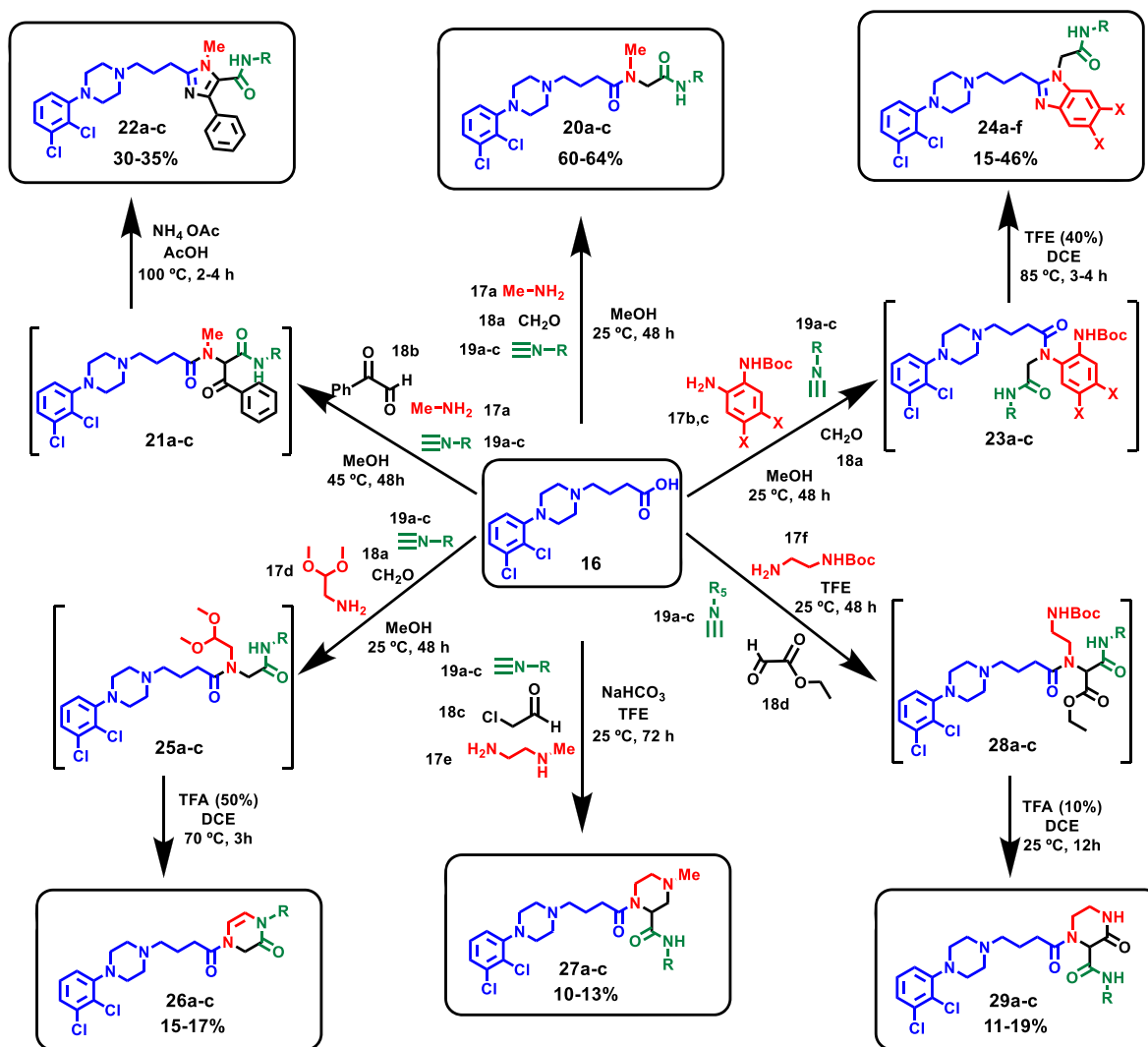
the exploration of alternative allosteric regions of the receptor (e.g., secondary pocket) adjacent to the primary (canonical) binding site. In other words, this conservative strategy could not deliver structurally novel ligands that are able to stabilize alternative conformational states of receptors.³⁹ Furthermore, most DRD₂ biased agonists developed to date do not show remarkable subtype selectivity toward the other receptors of the dopamine D₂ family (D₃ and D₄, Figure 1).⁴⁰ Evidence from clinical practice indicates that most effective antipsychotics exhibit a rather promiscuous receptor profile, with important affinity toward several GPCRs (usually defined as selectively nonselective drugs).^{41,42} However, from a chemical biology perspective, the development of molecular probes that simultaneously elicit subtype selectivity and signaling bias profiles is key to determine the molecular and physiological determinants that underpin DRD₂ biased signaling. Such pharmacological tools would contribute to our understanding of the molecular basis of DRD₂ signaling not only in transfected cells but also in complex and physiologically relevant environments. This information enables the elucidation of the real contribution of β -arrestin and G-protein signaling in dopaminergic receptors and the development of safer and more effective medications for schizophrenia and Parkinson's disease.

To overcome the limitations of previous approaches, we herein report the design, synthesis, and pharmacological characterization of several series of DRD₂ partial agonists that exhibit either G-protein or β -arrestin biased signaling profiles, uniquely combined with exquisite subtype selectivity. The new families of compounds were designed and assembled by using a highly versatile multicomponent approach. The experimental data provided structure–activity relationship (SAR) and structure–functional selectivity relationship (SFSR) trends that were consistent with the proposed binding modes, as defined in a receptor-driven docking model. The overall results of the study represent a successful proof-of-concept of an unexplored strategy for the rapid identification of novel structurally diverse and functionally selective DRD₂ ligands.

RESULTS AND DISCUSSIONS

Design and Synthesis. From a structural point of view, most studied DRD₂ biased ligands fit in the pharmacophoric model presented in Figure 2. These compounds are bitopic

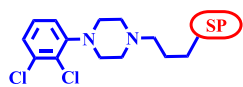
Scheme 1. Ugi-Based Assembly of the Target Compounds



ligands, containing three well-defined regions:⁴³ (1) the primary pharmacophore (PP) [commonly referred to as the left-hand side (LHS) or head group], consisting of a mono- or disubstituted phenyl-piperazine scaffold, (2) the central linker, that is usually variable in length and nature (e.g., acyclic or cyclic), and (3) the secondary (or allosteric) pharmacophore (SP) [commonly referred to as the right-hand side (RHS) or tail group], generally consisting of a heterocyclic core. Although the aromatic piperazines of the primary pharmacophore (PP) dictate the efficacy profile and is sufficient to allow binding to the primary (orthosteric) binding site of DRD_2 (and to that of the closely related DRD_3 subtype), enlargement of the chemical structures by addition of a flexible linker and a second, mostly lipophilic system (SP) has been found to promote enhanced affinity and subtype selectivity.^{44,45} In the present study, it was decided to maintain the primary pharmacophore (Figure 2), with the 1-(2,3-dichlorophenyl)-piperazine moiety selected (which is present in aripiprazole), and a shorter than usual (four atoms) linear linker, which is present in UNC9995^{12,33} (Figure 1). Six previously unexplored secondary pharmacophoric (SP) groups (Figure 2) were proposed to examine the effect of these structural modifications on subtype selectivity (DRD_2 , DRD_3 , and DRD_4) and also their effect on the DRD_2 functional selectivity profile of

the novel ligands. The selected SP frameworks provide novel topologies, physicochemical features, and alternative binding modes that should enable the capture of diverse conformational states within the receptor. In addition to the heterocyclic and functional diversity introduced, some of the proposed SP fragments bear a stereogenic center within the heterocyclic framework (Scheme 1, compounds **27** and **29**), thus introducing stereochemical diversity that would enable the future investigation of scarcely explored stereoselective interactions within the SP region.

The appropriate decoration of targeted structures (Figure 2), according to the specific requirements of the target receptor, would allow effective interaction with subpockets in the secondary (allosteric) binding site, ultimately resulting in optimized bioactivity levels. Moreover, the achievement of such decorations by synthetically feasible approaches is an emerging criterion for library design. The implementation of concise and efficient synthetic methodologies that reconcile molecular complexity with experimental simplicity, thus allowing rapid access to privileged molecular frameworks, constitutes a highly desirable goal within the competitive environment of drug discovery. A valuable addition to the compendium of preparative methods to generate drug candidate libraries is provided by multicomponent reactions

Table 1. Structures and Pharmacological Data at the D₂ Receptor Family for the Ligands^{a,b}


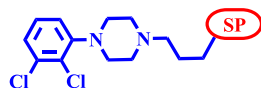
cAMP Functional data at the D₂-like receptor family^{a,b}

Cmpd	Secondary Pharmacophore (SP)	R	X	hD ₂		hD ₃		hD ₄	
				pIC ₅₀	%E _{max}	pIC ₅₀	%E _{max}	pIC ₅₀	%E _{max}
20a			-	8.34 ± 0.60	55 ± 4	5.24 ± 0.50	125 ± 5	6.79 ± 0.45	48 ± 10
20b			-	8.54 ± 0.42	45 ± 4	4.91 ± 1.37	128 ± 5	5.13 ± 0.81	82 ± 6
20c			-	5.81 ± 0.45	65 ± 5	5.64 ± 0.55	65 ± 4	4.86 ± 1.41	109 ± 6
22a			-	8.30 ± 0.38	60 ± 5	5.63 ± 0.33	98 ± 3	5.46 ± 0.72	101 ± 7
22b			-	5.76 ± 0.43	83 ± 8	6.11 ± 0.26	86 ± 8	5.64 ± 0.27	103 ± 10
22c			-	6.79 ± 0.56	73 ± 5	5.72 ± 0.42	80 ± 5	8.24 ± 0.50	72 ± 4
24a			H	4.87 ± 0.69	164 ± 4	4.42 ± 0.10	288 ± 5	5.00 ± 0.51	148 ± 3
24b			H	5.04 ± 0.88	92 ± 3	7.94 ± 0.42	20 ± 9	4.80 ± 1.20	93 ± 10
24c			H	6.43 ± 0.41	55 ± 8	6.40 ± 0.21	65 ± 6	8.10 ± 0.36	53 ± 9
24d			Br	8.66 ± 0.63	55 ± 5	4.63 ± 0.56	214 ± 3	8.01 ± 0.41	65 ± 6
24e			Br	5.42 ± 0.57	104 ± 3	5.64 ± 0.28	82 ± 3	6.89 ± 0.30	65 ± 8
24f			Br	6.35 ± 0.50	66 ± 5	5.59 ± 0.37	107 ± 3	5.58 ± 0.38	120 ± 4
26a			-	5.86 ± 0.26	88 ± 7	5.43 ± 0.26	111 ± 6	5.24 ± 1.25	95 ± 6
26b			-	6.96 ± 0.23	68 ± 8	5.49 ± 0.46	97 ± 7	5.89 ± 0.60	55 ± 5
26c			-	5.76 ± 0.30	113 ± 7	8.47 ± 1.26	66 ± 4	5.94 ± 0.13	80 ± 10
27a			-	8.96 ± 1.37	47 ± 4	4.80 ± 0.80	171 ± 8	5.04 ± 0.51	109 ± 8
27b			-	8.78 ± 0.79	60 ± 5	5.83 ± 0.57	93 ± 5	5.22 ± 1.40	54 ± 5
27c			-	5.83 ± 0.49	77 ± 9	5.25 ± 0.92	73 ± 7	5.26 ± 0.24	68 ± 9
29a			-	8.94 ± 1.16	62 ± 9	6.30 ± 0.42	86 ± 4	6.06 ± 0.42	53 ± 8
29b			-	5.48 ± 0.52	104 ± 3	4.57 ± 0.17	290 ± 4	5.16 ± 0.20	155 ± 3
29c			-	8.42 ± 0.85	58 ± 5	5.22 ± 0.21	146 ± 5	5.18 ± 0.53	83 ± 8
	Quinpirole			8.58 ± 0.11	100 ± 5	7.57 ± 0.14	100 ± 3	7.48 ± 0.07	100 ± 6

^apIC₅₀ and E_{max} values are the average of five experiments, each performed in duplicate with ± SEM values that are three times lower than the average. E_{max} relative to the effect of the reference agonist quinpirole. ^bTested using the experimental protocols described in the Experimental Section.

(MCRs),^{46,47} which have emerged as a tailored synthetic paradigm in the context of medicinal chemistry and chemical biology programs. MCRs combine three major principles in organic synthesis: convergence and atom and step economies. In addition, such reactions are highly flexible and their extraordinary exploratory power allows maximum structural complexity to be generated from simple starting materials in just a single step.⁴⁸ The main goal of the study reported here was to identify novel DRD₂ biased agonists by introducing unexplored structural elements in the secondary pharmacophore (SP) region. The selection criteria for the proposed SP groups were guided by the principles of synthetic feasibility and structural diversity (Figure 2). Thus, we envisioned different divergent, highly exploratory, and experimentally simple MCR-assisted pathways (Scheme 1). The selected synthetic approaches, which are based on the Ugi four-component reaction (U-4CR), exploit the potential of this transformation for structural diversification. Thus, starting from the readily available carboxylic acid **16**, which contains the primary pharmacophoric moiety and the linker, we envisioned a set of reactions (Scheme 1) in which **16** would be combined with diversely functionalized amine inputs (**17**), carbonyl partners (**18**), and three representative isocyanides (**19**).

The simplest set of ligands (**20a–c**) was obtained by the Ugi reaction of **16** with methylamine (**17a**), formaldehyde (**18a**), and isocyanides **19a–c** in methanol at room temperature for 48 h.⁴⁷ The assembly of the other five subsets (**22**, **24**, **26**, **27**, and **29**) involved the use of polyfunctional reactive substrates and/or the versatility of the Ugi-Deprotect-Cyclize (UDC) strategy.^{47,49,50} As shown in Scheme 1, the feasibility of the selected pathways relies heavily on the latent reactivity of the different functionalized Ugi adducts (**21**, **23**, **25**, and **28**), which, upon direct cyclization (**22**, **26**, and **27**) or removal of the protecting group, undergo an intramolecular cyclization (**24** and **29**) to furnish the target structures in an efficient transformation that takes place in one pot. In this way, compounds **22a–c** were obtained by reaction of **16** with methylamine (**17a**), isocyanides **19a–c**, and phenylglyoxal (**18b**) as the key precursor (Scheme 1). The superior reactivity of the formyl group in **18b** ensured the chemoselectivity of the reaction to produce an Ugi adduct (**21a–c**) that contains an enolizable ketone group, and this was transformed *in situ* to give **22a–c** by treatment with ammonium acetate at 100 °C.⁵¹ Treatment of the carboxylic acid **16** with formaldehyde (**18a**), isocyanides **19a–c**, and the mono-BOC protected phenylenediamines **17b–c** afforded the Ugi adducts **23**, which, upon acidic BOC cleavage and thermal treatment, afforded **24a–f**.

Table 2. Ligands and Structure–Selectivity Relationship (SSR) Data for Selected Ligands^{a,b}

Compd	Secondary Pharmacophore (SP)	D ₂ cAMP Inhibition		D ₃ cAMP Inhibition		D ₄ cAMP Inhibition		D ₂ β-Arrestin		Bias factor ^c cAMP - β-Arr ΔΔlog(<i>f</i> / <i>K_A</i>)
		pIC ₅₀ ± SEM	E _{max} ± SEM (%)	pIC ₅₀ ± SEM	E _{max} ± SEM (%)	pIC ₅₀ ± SEM	E _{max} ± SEM (%)	pEC ₅₀ ± SEM	E _{max} ± SEM (%)	
20a		8.34 ± 0.60	55 ± 4	5.24 ± 0.50	125 ± 5	6.79 ± 0.45	48 ± 10	8.49 ± 0.30	122 ± 2	-0.446
20b (ISAM-A13)		8.54 ± 0.42	45 ± 4	4.91 ± 1.37	128 ± 5	5.13 ± 0.81	82 ± 6	8.63 ± 0.31	129 ± 2	-0.508
22a (ISAM-A1684)		8.30 ± 0.38	60 ± 5	5.63 ± 0.33	98 ± 3	5.46 ± 0.72	101 ± 7	5.30 ± 1.05	*	2.223
24d (ISAM-A18)		8.66 ± 0.69	55 ± 5	4.63 ± 0.56	214 ± 3	8.01 ± 0.41	65 ± 6	5.50 ± 1.46	*	2.768
27a (ISAM-A51)		8.96 ± 1.37	47 ± 4	4.80 ± 0.80	171 ± 8	5.04 ± 0.51	109 ± 8	9.67 ± 0.62	93 ± 1	-0.977
27b		8.78 ± 0.79	60 ± 5	5.83 ± 0.57	93 ± 5	5.22 ± 1.94	54 ± 5	8.44 ± 0.25	120 ± 1	0.079
29a (ISAM-A53)		8.94 ± 1.16	62 ± 9	6.30 ± 0.42	86 ± 4	6.06 ± 0.42	53 ± 8	8.12 ± 0.20	142 ± 1	0.502
29c (ISAM-A52)		8.42 ± 0.85	58 ± 5	5.22 ± 0.21	146 ± 5	5.18 ± 0.53	83 ± 8	9.43 ± 0.57	68 ± 2	-1.043
Aripiprazole	-	7.42 ± 0.17	74 ± 4	7.09 ± 0.17	115 ± 4	5.93 ± 0.46	151 ± 3	9.00 ± 0.30	128 ± 2	-1.774
Quinpirole	-	8.75 ± 0.11	100 ± 5	7.57 ± 0.14	100 ± 3	7.48 ± 0.07	100 ± 6	8.61 ± 0.12	100 ± 1	0.000

^aEC₅₀, IC₅₀, and E_{max} values are the average of five experiments, each performed in duplicate with ± SEM values that are 3-fold less than the average. E_{max} relative to the effect of the reference agonist quinpirole. ^bTested using the experimental protocols described in the [Experimental Section](#). ^cBias factors were quantified by the operational model using quinpirole as a positive control (see the [Experimental Section](#)). Ligand bias values >0 indicate preference for the cAMP pathway, and values < 0 indicate preference for the β-arrestin signaling pathway. Values above 0.5 are considered significant and are highlighted. *E_{max} is not shown due to low affinity of the ligand.

(Scheme 1).⁵² The Ugi reaction of **16**, formaldehyde (**18a**), isocyanides **19a–c**, and aminoacetaldehyde dimethyl acetal (**17d**) generated the adducts **25**, which were transformed *in situ* to **26a–c** by an acid-mediated transformation that involved an intramolecular cyclization and subsequent elimination (Scheme 1).⁵³

The four-component reaction of **16**, isocyanides **19a–c**, and the bifunctional precursors **18c** (chloroacetaldehyde) and **17e** (*N*-methylethylenediamine) under basic conditions (NaHCO₃) directly afforded the piperazine derivatives **27a–c** (Scheme 1).⁵⁴ The sequence involves the formation of an Ugi adduct, which, under basic conditions, undergoes an intramolecular nucleophilic substitution reaction. Finally, the assembly of piperazin-2-ones **29a–c** was accomplished by a similar pathway (Scheme 1), starting from carboxylic acid **16** and isocyanides **19a–c**, but using two alternative bifunctional precursors [i.e., ethyl glyoxylate (**18d**) and *N*-BOC-ethylenediamine (**17f**)]. Acid-mediated cleavage of the BOC group in the Ugi adducts **28** provided the target ligands (**29**).⁵⁵ Ligands of series **27** and **29**, which contain a stereocenter within the SP heterocyclic fragment, were isolated and evaluated as racemic mixtures. A detailed description of the synthetic methods and the complete structural, spectroscopic, and analytical data for all compounds are provided in the [Experimental Section](#).

The five heterocyclic cores explored as secondary pharmacophoric groups (**22**, **24**, **26**, **27**, and **29**) can be considered as conformationally restricted analogs of the early

acyclic series **20**, with differences in structure, topology, physicochemical descriptors, and complexity. Thus, the Ugi-based diversification strategy enables the rapid differentiation of the structural elements of the acyl-aminoamide scaffold into highly diverse molecular frameworks.

Biological Evaluation. The newly synthesized ligands were all initially tested in cAMP inhibition assays with three dopamine receptor subtypes (DRD₂, DRD₃, and DRD₄), i.e., the DRD₂-like receptors, to evaluate their functional behavior and selectivity profile (Table 1). All experiments were performed *in vitro* on transfected HEK-293T cells, with the evaluation of the efficacy (E_{max}) and half maximum inhibitory concentration (IC₅₀) for the cAMP assays, using previously described experimental protocols.⁵⁶ Quinpirole was used as a control and reference drug during these studies. Compounds **27a–c** and **29a–c** were tested as racemic mixtures.

On the basis of its DRD₂ potency (pIC₅₀ > 8) and subtype selectivity criteria, seven ligands (**20a**, **20b**, **22a**, **27a**, **27b**, **29a**, and **29c**) were selected for further investigation of the DRD₂-mediated potency (EC₅₀) and efficacy (E_{max}) for β-arrestin-2 recruitment (Table 2). As a consequence of its excellent DRD₂ potency (pIC₅₀ = 8.66), albeit without selectivity toward DRD₄, ligand **24d** was also included in the set of compounds selected for bias characterization. The β-arrestin-2 recruitment study involved BRET experiments performed on transfected HEK-293T cells using previously described experimental protocols.⁵⁷ Aripiprazole and quinpirole were employed as controls during these studies.

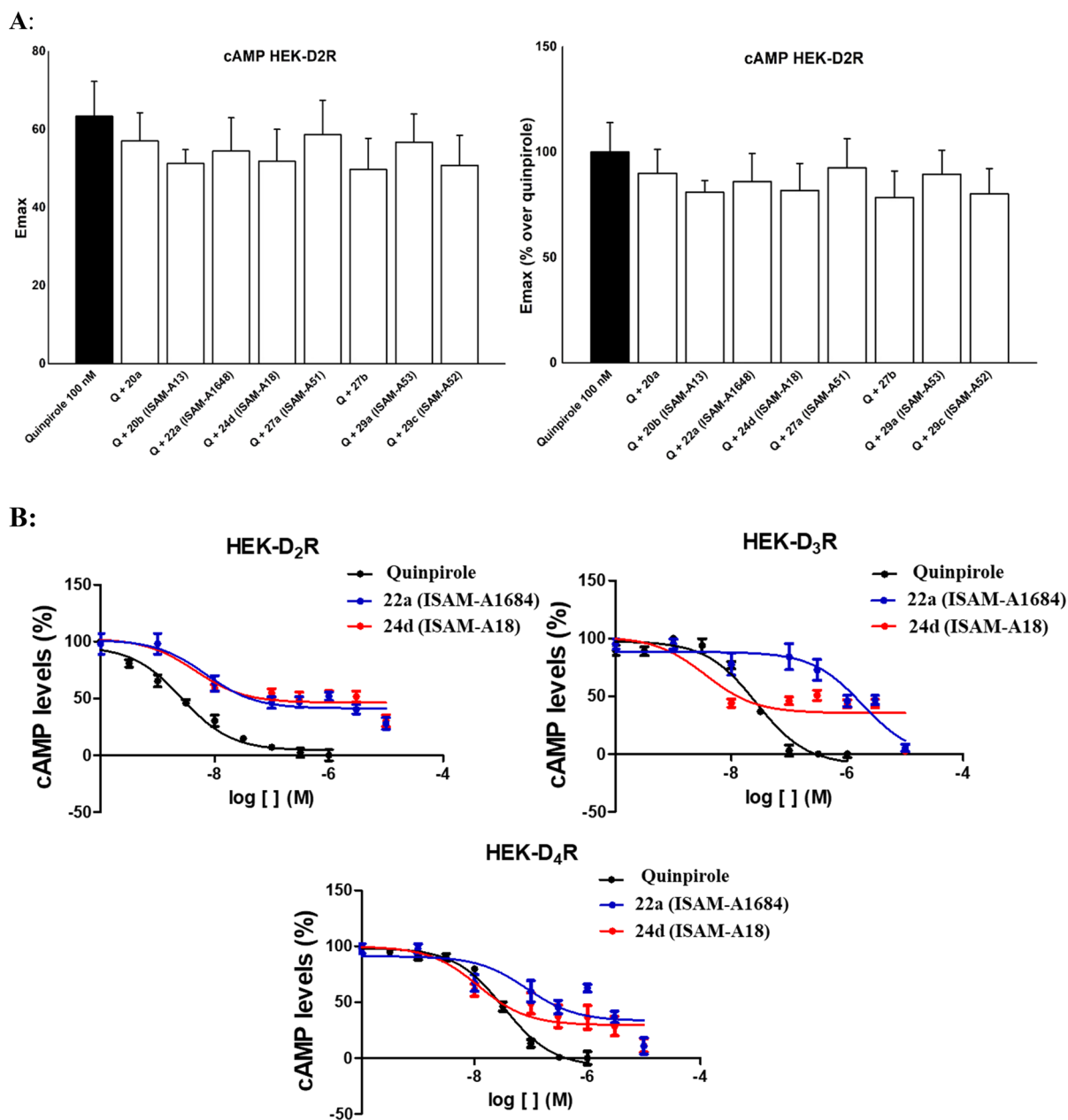


Figure 3. (A) E_{max} values for 100 nM quinpirole in cAMP assays performed in HEK-293T cells expressing DRD₂, pretreated or not (reference black column) with 100 nM of the selected compounds. Data are normalized (right) to the effect of quinpirole alone (100%). (B) HEK-293T cells expressing human DRD₂, DRD₃, or DRD₄ were treated with the indicated compounds. The effect of the compounds on the decrease of 500 nM-induced cAMP levels was determined as described in the Experimental Section. Data are given relative to the value of forskolin alone and then normalized to the effect of quinpirole.

With the aim of better exploring the pharmacological profile of the novel series herein documented it was decided to evaluate a set of ligands (Table 2, 20a, 20b, 22a, 24d, 27a, 27b, 29a, and 29c) in antagonist mode. In this case, cells were pretreated with the selected compounds before treatment with the agonist quinpirole (see Methods). As can be observed in Figure 3A, there were no significant variations in the efficacy between each of the compounds tested with quinpirole compared to the quinpirole tested alone. These results enable to discard a potential antagonistic behavior for the studied compounds. Figure 3B shows a comparative profile of the cAMP dose response curves obtained for ligands 22a and 24d and quinpirole at DRD₂, DRD₃, and DRD₄.

Structure–Activity and Structure–Selectivity Relationships. The cAMP functional data for the novel compounds (Table 1) reveal that some ligands behave as DRD₂ selective partial agonists. Inspection of reported data enables to identify eight novel and highly potent ($pIC_{50} > 8$) DRD₂ ligands (e.g., 20a, 20b, 22a, 24d, 27a, 27b, 29a, and 29c), six of which elicit remarkable selectivity (>1000-fold) toward DRD₃ and DRD₄. Furthermore, some potent and selective DRD₃ (i.e., 24b and 26c, $pIC_{50} = 7.94$ and 8.47, respectively) or DRD₄ (i.e., 22c and 24c, $pIC_{50} = 8.24$ and 8.10, respectively) ligands were identified. These data emphasize the potential of herein disclosed MCR-based diversification of the secondary pharmacophore region has in modulating the interaction with DRD₂. Additionally, our

results exemplify how subtle structural modifications on the secondary pocket can provoke important differentiation in the biological profile of the synthesized ligands.

For a more immediate and efficient analysis of the variation of both affinity and selectivity, the pIC_{50} values at DRD₂ (X axis) versus DRD₃ (Y axis, top panel) and DRD₄ (Y axis, bottom panel) are provided as independent scatter plots using the same scale and range for both axes (square plot). Each subset was represented in a different color and shape in order to facilitate a more comprehensive analysis of both potency and selectivity within a series. In both plots, the DRD₂ selective compounds appear below the diagonal (right bottom zone), with the distance from the diagonal being proportional to the degree of selectivity, confirming that the identified DRD₂ partial agonists also show a high degree of selectivity versus DRD₃/DRD₄. This subset was selected for further pharmacological characterization (see Table 2).

The functional data presented in Table 1 highlight the relevance of the amide group in the secondary pharmacophore for effective interaction within DRD₂. The only subset that did not provide potent DRD₂ ligands (26) has this amide group embedded within the heterocyclic core, which means that they lacked the polar hydrogen and had a conformational restraint, while the rest of the series provided at least one ligand with significant DRD₂ potency. In contrast to the low affinity on the DRD₂, series 26 provided compound 26c, a highly potent ($pIC_{50} = 8.47$) and selective (>300-fold) novel DRD₃ partial agonist.

Series 20, 27, and 29 generally yielded potent and subtype-selective DRD₂ partial agonists, and these included the most attractive ligands identified in this study (Table 1 and Figure 4). In these series, compounds bearing a benzyl group on the amide moiety (20a, 27a, and 29a) systematically exhibited a low nanomolar potency ($pIC_{50} = 8.34, 8.96,$ and 8.94 respectively). In contrast, the cyclohexyl group seems to be well tolerated only in acyl-aminoamides (20b) and the *N*-methylpiperazines (27b). Conversely, those compounds that contained a *tert*-butyl residue generated ligands (20c and 27c) that systematically exhibited micromolar potency, apart from 29c, thus suggesting that this group could not facilitate optimal complementarity within DRD₂. Although most ligands with imidazole- or benzimidazole-based SP groups (Table 1, ligands 22 and 24) have low potency at DRD₂, the pIC_{50} values determined for ligands 22a and 24d ($pIC_{50} = 8.30$ and 8.66 , respectively) reveal that these scaffolds, when appropriately decorated on the exocyclic amide group (i.e., with a benzyl group), can provide potent and selective DRD₂ partial agonists.

As previously discussed, 1-acyl-*N*-methylpiperazine-2-carboxamides 27 and 1-acyl-*N*-methyl-3-oxopiperazine-2-carboxamides 29 can be considered as conformationally restricted analogs of the acyl-aminoamides 20. Thus, their similar biological profile (potency and selectivity) could be a consequence of the close structural similarity of these three series. Despite the structural analogy, the cyclic constrained analogs (piperazine-2-carboxamides 27 and 3-oxopiperazine-2-carboxamides 29) exhibited slightly superior potency (Table 1) when compared to the acyclic series (20). This trend suggests that the cyclic derivatives are more similar to the bioactive conformation. As observed in the early series, and with the exception of 29c ($pIC_{50} = 8.42$), ligands bearing the *tert*-butyl group in the exocyclic amide afforded the weakest potency ($pIC_{50} = 5.76$ – 6.79). Another interesting structural feature of the conformationally restricted series 27 and 29 is

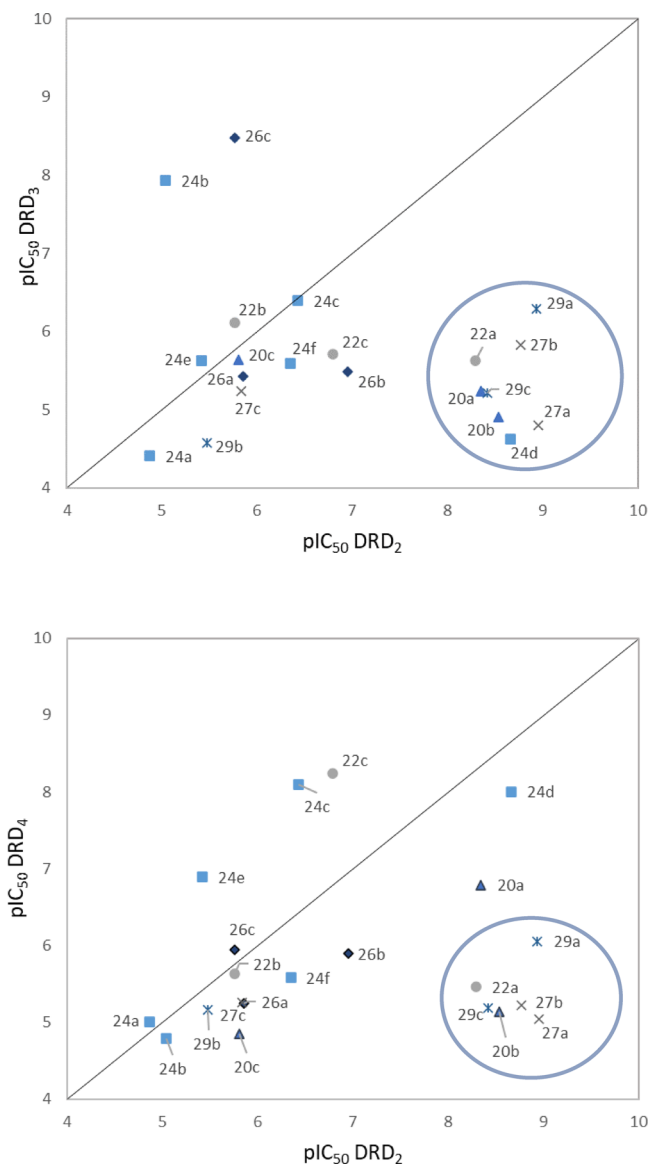


Figure 4. Potency–selectivity DRD₃–DRD₂ and DRD₄–DRD₂ plots.

the presence of a stereogenic center at position 2 of the heterocyclic core. Although these compounds were tested as racemates, it is reasonable to expect diverse pharmacological profiles for the different enantiomers. Accordingly, the potential influence of the absolute configuration of the stereogenic center in these series will be explored in future work.

DRD₂-mediated signaling events are initiated either by G protein-dependent (G-protein-coupled) and/or G protein-independent pathways (β -arrestin recruitment). The ability of a (partial) agonist to selectively activate one of these specific signaling pathways is a pharmacological phenomenon known as functional bias (or functional selectivity). A key goal of this study was to explore the relationship between the biased selectivity and the structural features of the ligand, which ultimately lead to the establishment of specific interactions with DRD₂. Thus, we selected the seven derivatives (20a, 20b, 22a, 27a, 27b, 29a, and 29c) that exhibited a high cAMP potency ($pIC_{50} > 8$) and optimal DRD₂ selectivity (Table 1) to perform a β -arrestin-2 recruitment BRET assay in transfected HEK-293T cells, which determines the potency and efficacy

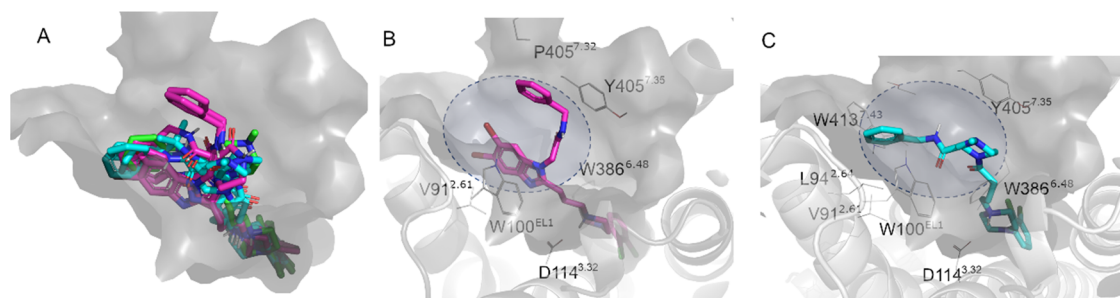


Figure 5. Binding mode of compounds in Table 2 on the inactive DRD₂, PDB code 6CM4 (A). Compounds are color coded according to their pharmacological activity as G-protein biased (magenta), β -arrestin biased (cyan), or no bias (green). The detailed binding mode for each compound class is shown, for compound 24d (B) and compound 27a (C), depicting the residues involved in interactions with the ligand in each case, and the variable region occupied by the SP designated with a blue circle.

for β -arrestin-2 recruitment. Although it was not selective (DRD₄ pIC₅₀ = 8.01), the benzimidazole derivative 24d was included in this study due to its excellent DRD₂ potency (pIC₅₀ = 8.66). Aripiprazole, a known biased ligand, was used as a reference ligand and quinpirole⁵⁸ (a full agonist of DRD₂) was used as a positive control in both cAMP and β -arrestin-2 recruitment BRET assays. The comparative cAMP and β -arrestin-2 data are presented in Table 2. In order to identify functional bias rapidly, a bias factor was calculated using the Black and Leff operational model⁵⁹ with respect to quinpirole (see Table 2). Most of the evaluated ligands exhibited excellent efficacy in the β -arrestin recruitment pathway (E_{max} over quinpirole in the range 68–142%, see Table 2), thus behaving as full agonists for this pathway. The most salient data emerging from β -arrestin recruitment assays evidenced two pairs of ligands that elicit opposite signaling profiles. Thus, while ligands 27a and 29c exhibit a very attractive sub-nanomolar profile in the β -arrestin recruitment test (pIC₅₀ = 9.67 and 9.43, respectively), derivatives 22a and 24d showed only weak potency (micromolar range). The availability of ligands bearing different groups on the exocyclic amide in series 20, 27, and 29 provided evidence of the key role of the alkyl group (benzyl, cyclohexyl, or *tert*-butyl) on the β -arrestin recruitment potency. Interestingly, the compounds that elicited the poorest β -arrestin recruitment potency (22a and 24d) contain an aromatic heterocyclic core with an *N*-benzyl group within the secondary pharmacophore.

Six of the ligands (20b, 22a, 24d, 27a, 29a, and 29c) showed a clear functional selectivity profile (biased agonism) according to the bias factor parameter (Table 2), where a positive value indicates a preference for the cAMP pathway and a negative value denotes that β -arrestin recruitment is dominant. As one would expect, the weak potency in the β -arrestin recruitment assay and excellent cAMP data mean that ligands 22a and 24d show a significant bias toward cAMP [$\Delta\Delta\log(\tau/K_A)$ = 2.223 and $\Delta\Delta\log(\tau/K_A)$ = 2.768, respectively]. These values represent 167-fold and 586-fold bias, respectively, toward the cAMP pathway. Furthermore, compound 29a also shows a moderate [$\Delta\Delta\log(\tau/K_A)$ = 0.502] 3-fold bias toward cAMP inhibition. In contrast, ligands 27a and 29c, due to their sub-nanomolar effect and excellent efficacy in the β -arrestin pathway (pEC₅₀ = 9.67 and 9.43, respectively) and its potency and moderate efficacy in the cAMP pathway, showed 10-fold and 11-fold β -arrestin biased agonism. Compound 24d, besides being one of the most potent binders at DRD₂ and indeed the partial agonist with strongest bias toward the cAMP pathway (Table 2), lacks the

required D₂/D₄ selectivity profile (Table 1) to warrant further characterization of this particular compound. In any case, compound 24d was used as a tool to understand the molecular basis of its biased profile.

In order to investigate the structural basis for the different biased signaling profiles, a complex of each of the molecules listed in Table 2 with DRD₂ was generated by different docking approaches, initially using the crystal structure of DRD₂ in complex with risperidone.⁶⁰ Despite the fact that this is an inactive conformation of the receptor, the chemical similarity of the general scaffold of our compounds with the co-crystallized antagonist (risperidone) supported the use of this crystal structure. Moreover, the orthosteric binding site of the aminergic receptor is not expected to change substantially upon complexation with partial agonists.⁶¹ As derived from the binding mode obtained (Figure 5), the 2,3-dichlorophenyl ring on the piperazine scaffold (primary pharmacophore, commonly referred to as LHS) is analogous to the benzisoxazole moiety of risperidone, which uniquely extends into a deep binding pocket defined by the side chains of residues in TM3 (Cys118^{3,36} and Ile122^{3,40}), TM5 (Ser197^{5,46} and Phe198^{5,47}), and TM6 (Phe382^{6,44}, Phe390^{6,52}, and Trp386^{6,48}) as opposed to other dopaminergic ligands crystallized to date.^{60,62,63} The common anchoring point throughout the series is the salt bridge interaction between the charged nitrogen in the piperazine and the sidechain of Asp114^{3,32}. The position of the secondary pharmacophore (SP) is, as expected, more variable. Interestingly, there is a correlation between the pharmacological activity and the structural features introduced, thus providing an initial proposal for the structural interpretation of ligand bias on this receptor. Thus, the two strongest G-protein biased ligands (22a and 24d, magenta in Figure 5) place the benzyl tail toward the extracellular region, thus making distinct contacts with the tip of TM7 (Pro405^{7,32} and Tyr408^{7,35}). This arrangement is in contrast to the other benzyl-containing SP, which were moderately selective for the β -arrestin signaling pathway (20a and 27a) and bend the SP toward TM2 (Val91^{2,61} and Leu94^{2,64}, ligands in cyan in Figure 5). A similar orientation was found for the cyclohexyl substituent in ligands 20b (β -arrestin-biased) and 27b (non-biased) or even for the benzyl-containing 29a, which shows a less pronounced bias toward the G-protein pathway. According to this model, imidazole- or benzimidazole-based SP groups, specifically decorated with the exocyclic amide benzyl substituted, occupy a distinct subpocket that might be related to their G-protein biased profile, while there is no clear specific subpocket for β -arrestin biased ligands. Additionally, this

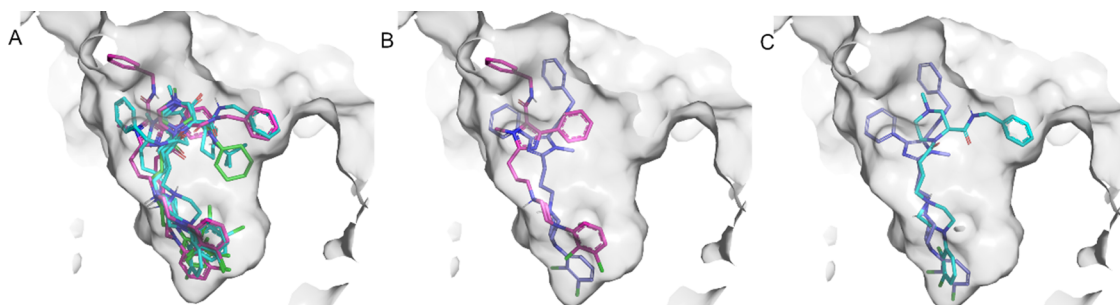


Figure 6. Binding mode of compounds in Table 2 on the active conformation of DRD₂, PDB code 6CMS (A). Compounds are color coded according to their pharmacological activity as in Figure 5. The comparison with the corresponding binding pose on the inactive conformation of DRD₂ is shown for compound 22a (G-protein biased, B) and compound 27a (β -arrestin biased, C).

binding mode agrees with the previous observations of the so-called extended binding domain (EBD) playing a role in the DR subtype specificity.^{60,62,63} The recent crystal structure of DRD₂ with the atypical antipsychotic haloperidol⁶⁴ demonstrated the flexible nature of this pocket, where the conserved Trp100 in EL1 can open a new space for the rigid substituent of this molecule, thus opening the door to a more comprehensive dynamic characterization of the binding mode of different DRD₂ ligands.

During the course of this study, a structure of the active DRD₂-G_i complex was revealed by cryo-EM.⁶⁵ Despite the moderate resolution (3.8 Å), the binding mode of the orthosteric agonist bromocriptine is well evidenced. While mostly superimposing with risperidone, the bromine substituent does not reach as deep in the binding pocket as in the case of the fluorine of the antagonist, while in the EBD, the bicyclic tripeptide group of this agonist relatively overlays with the tetrahydropyridopyrimidone of risperidone.⁶⁵ However, the differences in the conformation of the EL2 region between the two structures are notorious, favoring that the terminal part of the tripeptide in bromocriptine protrudes toward the extracellular tip of TM5. Consequently, an additional docking exploration of our compound series was performed using this active structure. Given the differences on the binding pocket of the head group, we had to impose additional flexibility during the docking exploration.⁶⁶ The results, shown in Figure 6, reveal moderate adaptations of the binding pose of each compound as compared to the dockings on the inactive conformation of the receptor, mainly due to the impossibility to protrude as deep in the active conformation cavity as they do in the inactive conformation of the DRD₂. Still, it is interesting that the G-protein biased ligand 22a orients its benzyl tail toward the extracellular region of TM7, analogously to the inactive-bound configuration of this ligand (Figure 6B). In contrast, non-biased and β -arrestin biased ligands mostly show an alternative configuration of the SP substituents.

Altogether, the binding mode of each compound to both active and inactive conformations of the receptor suggest that the specific arrangement of the secondary pharmacophore (SP) substituent could be the key feature to the pharmacological profile of the ligands. Another interesting outcome is that, independent of the pharmacological nature of the ligand, only the (*R*) stereoisomers in series bearing a stereogenic center (27–29) can bind the receptor while maintaining the common interactions for the common parts of the ligands. Both of these aspects, i.e., the potential stereospecificity and the molecular mechanism associated to the ligand bias, are currently under further investigation in our groups.

CONCLUSIONS

In summary, we have documented a previously unexplored multicomponent-based approach that enables the rapid generation of novel subtype-selective DRD₂ biased ligands. This strategy exemplifies the search for diverse and previously unexplored structural elements binding the secondary pharmacophore but also highlights their critical role in modulating the functional selectivity profile. The pharmacological characterization of the new series of compounds enabled the identification of several ligands that elicit excellent DRD₂ selectivity and remarkable functional selectivity by either the cAMP (22a and 29a) or β -arrestin (29c, 27a and 20b) signaling pathways. These results can to some extent be explained by the molecular modeling of these ligands using the recent DRD₂ experimental structures. Further studies are now in progress in our laboratory to expand the diversity of the PP, SP, and linkers, to explore in detail the SAR and SSR around ligands 22a, 29a, 29c, and 27a, and to establish the role of stereochemistry in the observed biological profiles.

EXPERIMENTAL SECTION

Chemistry. Unless stated otherwise, all starting materials, reagents and solvents were purchased and used without further purification. After extraction from aqueous phases, the organic solvents were dried over anhydrous sodium sulfate. The reactions were monitored by thin-layer chromatography (TLC) on 2.5 mm Merck silica gel GF 254 strips, and the purified compounds each showed a single spot, unless stated otherwise, UV light and/or iodine vapor were used for detection of compounds. The Ugi reactions were performed in coated Kimble vials on a PLS (6X4) Organic Synthesizer with orbital stirring. The purity and identity of all tested compounds were established by mass spectrometry, HRMS, and NMR spectra as described below. Purification of isolated products was carried out by column chromatography (Kieselgel 0.040–0.063 mm, E. Merck) or medium-pressure liquid chromatography (MPLC) on a CombiFlash Companion (Teledyne ISCO) with RediSep pre-packed normal-phase silica gel (35–60 μ m) columns. Melting points were determined on a Gallenkamp melting point apparatus and are uncorrected. NMR spectra were recorded on Bruker AM300 and XM500 spectrometers. Chemical shifts are given as δ values against tetramethylsilane as an internal standard, and *J* values are given in Hz. Mass spectra were obtained on a Varian MAT-711 instrument. High-resolution mass spectra were obtained on an Autospec Micromass spectrometer. Routine purity control was performed by analytical HPLC using an Agilent 1100 system using an Agilent Zorbax SB-Phenyl, 2.1 mm \times 150 mm, 5 μ m column with gradient elution using the mobile phases (A) H₂O containing 0.1% CF₃COOH and (B) MeCN and a flow rate of 1 mL/min. The purity of all tested compounds was determined to be >95%. A detailed description of synthetic methodologies as well as analytical and spectroscopic data for all described compounds are provided below.

General Procedure for the Synthesis of 4-(4-(2,3-Dichlorophenyl)piperazin-1-yl)-N-methylbutanamide Derivatives (20a–c). A mixture of 4-(4-(2,3-dichlorophenyl)piperazin-1-yl)butanoic acid **16** (0.58 mmol), formaldehyde **18a** (0.58 mmol), methylamine **17a** (0.58 mmol), and the corresponding isocyanide (**19a–c**) (0.58 mmol, 1. eq) in methanol (2 mL) was stirred at 25 °C for 48 h. The reaction was monitored by TLC. After completion of the reaction, PS-*p*-TsOH (2.0 mmol) and CH₂Cl₂ (3 mL) were added. The reaction mixture was submitted to orbital stirring at room temperature until complete consumption of the unreacted isocyanide (30–60 min). The polystyrene-supported salt was filtered off and successively washed with MeOH (3 × 5 mL) and CH₂Cl₂ (3 × 5 mL). To the polystyrene-supported salt was added CH₂Cl₂ (3 mL) and DIPEA (3.0 eq), and the mixture was submitted to orbital stirring at room temperature for 60 min. Solvents were combined and evaporated to dryness. The resulting oil was purified by column chromatography on silica gel using MeOH/CH₂Cl₂.

N-(2-(Benzylamino)-2-oxoethyl)-4-(4-(2,3-dichlorophenyl)piperazin-1-yl)-N-methylbutanamide (20a). Yield: 64%. Mp: 88–90 °C. ¹H NMR (300 MHz, CDCl₃) δ (ppm): 7.36–7.20 (m, 5H), 7.19–7.08 (m, 2H), 6.99–6.88 (m, 1H), 6.67 (bs, 1H), 4.43 (d, *J* = 5.8 Hz, 2H), 4.04 (s, 2H), 3.14 (s, 3H), 3.04 (bs, 4H), 2.61 (bs, 4H), 2.49–2.38 (m, 4H), 1.98–1.75 (m, 2H). ¹³C NMR (75 MHz, CDCl₃) δ (ppm): 174.1, 169.1, 151.3, 138.3, 134.2, 128.8, 128.8, 127.8, 127.8, 127.7, 127.7, 127.6, 124.7, 118.7, 57.7, 53.3, 53.3, 52.9, 51.3, 51.3, 43.5, 37.1, 30.9, 22.1. HRMS (CI) *m/z* calcd for C₂₄H₃₁Cl₂N₄O₂ [M + H]⁺: 477.1824, found: 477.1840.

N-(2-(Cyclohexylamino)-2-oxoethyl)-4-(4-(2,3-dichlorophenyl)piperazin-1-yl)-N-methylbutanamide (20b). Yield: 63%. Mp: 124–126 °C. ¹H NMR (300 MHz, CDCl₃) δ (ppm): 7.18–7.08 (m, 2H), 6.94 (dd, *J* = 6.3, 3.2 Hz, 1H), 6.20 (bs, 1H), 3.96 (s, 2H), 3.79–3.65 (m, 1H), 3.12 (s, 3H), 3.07 (s, 4H), 2.67 (bs, 4H), 2.52–2.41 (m, 4H), 1.94–1.80 (m, 4H), 1.76–1.52 (m, 2H), 1.46–1.04 (m, 6H). ¹³C NMR (75 MHz, CDCl₃) δ (ppm): 173.9, 168.2, 151.3, 139.0, 134.2, 127.7, 124.8, 118.7, 57.7, 53.4, 53.3, 53.0, 51.3, 51.3, 48.2, 33.3, 33.1, 33.0, 30.9, 25.6, 24.8, 24.8, 22.1. HRMS (CI) *m/z* calcd for C₂₃H₃₅Cl₂N₄O₂ [M + H]⁺: 469.2137, found: 469.2137.

N-(2-(tert-Butylamino)-2-oxoethyl)-4-(4-(2,3-dichlorophenyl)piperazin-1-yl)-N-methylbutanamide (20c). Yield: 60%. Mp: 93–94 °C. ¹H NMR (300 MHz, CDCl₃) δ (ppm): 7.14–7.07 (m, 2H), 6.91 (dd, *J* = 5.9, 3.8 Hz, 1H), 6.04 (bs, 1H), 3.86 (s, 2H), 3.09 (s, 3H), 3.02 (bs, 4H), 2.61 (bs, 4H), 2.48–2.36 (m, 4H), 1.93–1.76 (m, 2H), 1.29 (s, 9H). ¹³C NMR (75 MHz, CDCl₃) δ (ppm): 173.7, 168.3, 151.3, 134.0, 127.5, 127.5, 124.6, 118.7, 57.6, 53.4, 53.2, 51.3, 51.2, 36.9, 30.8, 28.8, 22.1. HRMS (CI) *m/z* calcd for C₂₁H₃₃Cl₂N₄O₂ [M + H]⁺: 443.1981, found: 443.1984.

General Procedure for the Synthesis of 2-(3-(4-(2,3-Dichlorophenyl)piperazin-1-yl)propyl)-1-methyl-4-phenyl-1H-imidazole-5-carboxamide Derivatives (22a–c). A mixture of 4-(4-(2,3-dichlorophenyl)piperazin-1-yl)butanoic acid **16** (0.47 mmol), phenylglyoxal **18b** (0.47 mmol), methylamine **17a** (0.47 mmol), and the corresponding isocyanide (**19a–c**) (0.47 mmol) in trifluoroethanol (2 mL) was stirred at 45 °C for 48 h. The reaction was monitored by TLC. After completion of the reaction, PS-*p*-TsOH (2.0 mmol) and CH₂Cl₂ (3 mL) were added. The reaction mixture was submitted to orbital stirring at room temperature until complete consumption of the unreacted isocyanide (30–60 min). The polystyrene-supported salt was filtered off and successively washed with MeOH (3 × 5 mL) and CH₂Cl₂ (3 × 5 mL). To the polystyrene-supported salt was added CH₂Cl₂ (3 mL) and DIPEA (3.0 eq), and the mixture was submitted to orbital stirring at room temperature for 60 min. The solvents were combined and evaporated to dryness. The residue was dissolved in acetic acid (4 mL), NH₄OAc (18.8 mmol, 40 eq) was added, and the reaction was stirred at 100 °C for 2–4 h. After completion of the reaction, the mixture was neutralized with a saturated aqueous NaHCO₃ and extracted with AcOEt (2 × 10 mL) and CH₂Cl₂ (2 × 10 mL). The organic layers were combined and dried with Na₂SO₄, and the resulting oil was purified by column chromatography on silica gel using MeOH/CH₂Cl₂.

N-Benzyl-2-(3-(4-(2,3-dichlorophenyl)piperazin-1-yl)propyl)-1-methyl-4-phenyl-1H-imidazole-5-carboxamide (22a). Yield: 35%.

Mp: 145–147 °C. ¹H NMR (300 MHz, CDCl₃) δ (ppm): 7.51–7.42 (m, 2H), 7.32–7.22 (m, 6H), 7.19–7.07 (m, 4H), 6.94 (dd, *J* = 6.7, 2.9 Hz, 1H), 5.95 (t, *J* = 6.0 Hz, 1H), 4.42 (d, *J* = 5.9 Hz, 2H), 3.88 (s, 3H), 3.05 (bs, 4H), 2.81 (t, *J* = 7.6 Hz, 2H), 2.65 (bs, 4H), 2.54 (t, *J* = 7.1 Hz, 2H), 2.09–1.95 (m, 2H). ¹³C NMR (75 MHz, CDCl₃) δ (ppm): 161.2, 151.1, 150.8, 142.3, 141.5, 137.4, 134.0, 134.0, 129.5, 129.1, 129.0, 128.9, 128.7, 128.6, 128.2, 128.1, 127.9, 127.5, 127.4, 124.7, 122.2, 118.7, 66.2, 57.5, 53.1, 51.1, 43.5, 32.3, 24.7, 24.6. HRMS (CI) *m/z* calcd for C₃₁H₃₄Cl₂N₅O [M + H]⁺: 562.2140, found: 562.2147.

N-Cyclohexyl-2-(3-(4-(2,3-dichlorophenyl)piperazin-1-yl)propyl)-1-methyl-4-phenyl-1H-imidazole-5-carboxamide (22b). Yield: 30%. Mp: 140–142 °C. ¹H NMR (300 MHz, CDCl₃) δ (ppm): 7.59–7.52 (m, 2H), 7.44–7.32 (m, 3H), 7.17–7.12 (m, 2H), 6.95 (dd, *J* = 6.6, 3.0 Hz, 1H), 5.51 (d, *J* = 8.0 Hz, 1H), 3.89–3.78 (m, 4H), 3.06 (bs, 4H), 2.80 (t, *J* = 7.6 Hz, 2H), 2.67 (bs, 4H), 2.56 (t, *J* = 7.2 Hz, 2H), 2.10–1.94 (m, 2H), 1.86–1.71 (m, 2H), 1.60–1.47 (m, 3H), 1.40–1.21 (m, 2H), 1.16–0.80 (m, 3H). ¹³C NMR (75 MHz, CDCl₃) δ (ppm): 160.4, 151.1, 150.4, 141.6, 134.1, 134.0, 129.2, 129.0, 128.6, 128.2, 127.5, 124.6, 122.6, 118.6, 118.5, 57.5, 53.1, 51.1, 48.0, 32.4, 25.3, 24.8, 24.7, 24.5. HRMS (CI) *m/z* calcd for C₃₀H₃₈Cl₂N₅O [M + H]⁺: 554.2453, found: 554.2462.

N-(tert-Butyl)-2-(3-(4-(2,3-dichlorophenyl)piperazin-1-yl)propyl)-1-methyl-4-phenyl-1H-imidazole-5-carboxamide (22c). Yield: 33%. Mp: 86–88 °C. ¹H NMR (300 MHz, CDCl₃) δ (ppm): 7.60–7.49 (m, 2H), 7.47–7.29 (m, 3H), 7.19–7.08 (m, 2H), 6.95 (dd, *J* = 6.6, 2.9 Hz, 1H), 5.44 (bs, 1H), 3.83 (s, 3H), 3.07 (bs, 4H), 2.80 (t, *J* = 7.5 Hz, 2H), 2.68 (bs, 4H), 2.62–2.50 (m, 2H), 2.05–1.99 (m, 2H), 1.21 (s, 9H). ¹³C NMR (75 MHz, CDCl₃) δ (ppm): 160.8, 150.1, 134.2, 134.1, 132.1, 129.2, 128.7, 128.6, 128.2, 127.7, 127.5, 127.3, 126.1, 125.5, 118.9, 118.8, 76.8, 59.0, 52.9, 51.5, 49.8, 31.9, 28.5, 24.6, 22.7. HRMS (CI) *m/z* calcd for C₂₈H₃₆Cl₂N₅O [M + H]⁺: 528.2297, found: 528.2280.

General Procedure for the Synthesis of 2-(2-(3-(4-(2,3-Dichlorophenyl)piperazin-1-yl)propyl)-1-methyl-4-phenyl-1H-imidazole-5-carboxamide Derivatives (24a–f). A mixture of 4-(4-(2,3-dichlorophenyl)piperazin-1-yl)butanoic acid **16** (0.47 mmol), formaldehyde **18a** (0.47 mmol), mono-BOC protected phenylenediamines **17b–c** (0.47 mmol), and the corresponding isocyanide (**19a–c**) (0.47 mmol) in methanol (2 mL) was stirred at 25 °C for 48 h. The reaction was monitored by TLC. After completion of the reaction, PS-*p*-TsOH (2.0 mmol) and CH₂Cl₂ (3 mL) were added. The reaction mixture was submitted to orbital stirring at room temperature until complete consumption of the unreacted isocyanide (30–60 min). The polystyrene-supported salt was filtered off and successively washed with MeOH (3 × 5 mL) and CH₂Cl₂ (3 × 5 mL). To the polystyrene-supported salt was added CH₂Cl₂ (3 mL) and DIPEA (1.41 mmol), and the mixture was submitted to orbital stirring at room temperature for 60 min. Solvents were combined and evaporated to dryness. The residue was dissolved in a 40% solution of trifluoroacetic acid in dichloroethane, and the reaction mixture was stirred at 85 °C for 3–4 h. After completion of the reaction, the mixture was neutralized with a saturated solution of NaHCO₃, and the product was extracted with AcOEt (2 × 10 mL) and CH₂Cl₂ (2 × 10 mL). The organic layers were combined and dried with Na₂SO₄, and the resulting oil was purified by column chromatography on silica gel using MeOH/CH₂Cl₂.

N-Benzyl-2-(2-(3-(4-(2,3-dichlorophenyl)piperazin-1-yl)propyl)-1H-benzo[d]imidazol-1-yl)acetamide (24a). Yield: 15%. Mp: 95–97 °C. ¹H NMR (300 MHz, CDCl₃) δ (ppm): 7.75–7.65 (m, 1H), 7.33–7.18 (m, 6H), 7.17–7.07 (m, 4H), 6.90 (dd, *J* = 6.5, 3.1 Hz, 1H), 6.03 (t, *J* = 5.7 Hz, 1H), 4.88 (s, 2H), 4.40 (d, *J* = 5.9 Hz, 2H), 2.98 (bs, 4H), 2.83 (t, *J* = 7.5 Hz, 2H), 2.58 (bs, 4H), 2.46 (t, *J* = 6.8 Hz, 2H), 2.13–1.93 (m, 2H). ¹³C NMR (75 MHz, CDCl₃) δ (ppm): 166.7, 155.1, 151.1, 142.7, 137.3, 134.8, 134.0, 128.7, 127.7, 127.5, 124.7, 124.6, 123.2, 123.1, 122.9, 119.6, 118.7, 108.9, 57.2, 53.1, 51.1, 46.9, 43.4, 24.9, 24.4. HRMS (APCI) *m/z* calcd for C₂₉H₃₂Cl₂N₅O [M + H]⁺: 536.1975, found: 536.1978.

N-Cyclohexyl-2-(2-(3-(4-(2,3-dichlorophenyl)piperazin-1-yl)propyl)-1H-benzo[d]imidazol-1-yl)acetamide (24b). Yield: 36%.

Mp: 115–117 °C. ¹H NMR (300 MHz, CDCl₃) δ (ppm): 7.80–7.69 (m, 1H), 7.37–7.20 (m, 3H), 7.19–7.06 (m, 2H), 6.91 (dd, *J* = 6.6, 3.0 Hz, 1H), 5.25 (bs, 1H), 4.82 (s, 2H), 3.90–3.68 (m, 1H), 3.01 (bs, 4H), 2.90 (t, *J* = 6.5 Hz, 2H), 2.63 (bs, 4H), 2.54 (t, *J* = 6.8 Hz, 2H), 2.17–2.05 (m, 2H), 1.83–1.46 (m, 4H), 1.39–1.15 (m, 3H), 1.02–0.83 (m, 3H). ¹³C NMR (75 MHz, CDCl₃) δ (ppm): 165.6, 155.2, 151.1, 142.6, 134.8, 134.0, 127.5, 124.6, 123.1, 122.8, 119.5, 119.4, 118.6, 109.0, 57.2, 53.1, 51.2, 48.6, 47.0, 32.7, 25.2, 24.9, 24.7, 24.5. HRMS (CI) *m/z* calcd for C₂₈H₃₆Cl₂N₅O [*M* + *H*]⁺: 528.2297, found: 528.2292.

N-(*tert*-Butyl)-2-(2-(3-(4-(2,3-dichlorophenyl)piperazin-1-yl)propyl)-1*H*-benzo[d]imidazol-1-yl)acetamide (**24c**). Yield: 30%. Mp: 91–93 °C. ¹H NMR (300 MHz, CDCl₃) δ (ppm): 7.79–7.70 (m, 1H), 7.33–7.23 (m, 3H), 7.18–7.09 (m, 2H), 6.91 (dd, *J* = 6.4, 3.2 Hz, 1H), 5.17 (bs, 1H), 4.73 (s, 2H), 3.01 (bs, 4H), 2.91 (t, *J* = 7.0 Hz, 2H), 2.63 (bs, 4H), 2.54 (t, *J* = 6.9 Hz, 2H), 2.18–2.04 (m, 2H), 1.24 (s, 9H). ¹³C NMR (75 MHz, CDCl₃) δ (ppm): 165.8, 155.2, 151.2, 142.7, 134.8, 134.1, 127.6, 124.7, 123.1, 122.9, 119.7, 119.6, 118.7, 109.0, 57.4, 53.2, 52.0, 51.3, 47.6, 28.7, 25.1, 24.6. HRMS (CI) *m/z* calcd for C₂₆H₃₄Cl₂N₅O [*M* + *H*]⁺: 502.2140, found: 502.2127.

N-Benzyl-2-(5,6-dibromo-2-(3-(4-(2,3-dichlorophenyl)piperazin-1-yl)propyl)-1*H*-benzo[d]imidazol-1-yl)acetamide (**24d**). Yield: 43%. Mp: 208–210 °C. ¹H NMR (300 MHz, CDCl₃) δ (ppm): 7.96 (s, 1H), 7.56 (s, 1H), 7.35–7.27 (m, 3H), 7.19–7.13 (m, 4H), 6.89 (dd, *J* = 6.6, 3.0 Hz, 1H), 5.86 (bs, 1H), 4.83 (s, 2H), 4.44 (d, *J* = 5.9 Hz, 2H), 2.99 (bs, 4H), 2.86 (t, *J* = 7.4 Hz, 2H), 2.61 (bs, 4H), 2.50 (t, *J* = 6.5 Hz, 2H), 2.15–1.98 (m, 2H). ¹³C NMR (75 MHz, DMSO-*d*₆) δ (ppm): 166.4, 158.4, 151.2, 142.8, 138.9, 136.3, 132.6, 128.3, 127.3, 127.0, 126.0, 124.3, 122.6, 119.4, 115.6, 115.4, 114.8, 56.8, 52.7, 50.9, 45.8, 42.4, 24.4, 23.9. HRMS (CI) *m/z* calcd for C₂₉H₃₀Br₂Cl₂N₅O [*M* + *H*]⁺: 692.0194, found: 692.0186.

N-Cyclohexyl-2-(5,6-dibromo-2-(3-(4-(2,3-dichlorophenyl)piperazin-1-yl)propyl)-1*H*-benzo[d]imidazol-1-yl)acetamide (**24e**). Yield: 46%. Mp: 220–222 °C. ¹H NMR (300 MHz, CDCl₃) δ (ppm): 8.01 (s, 1H), 7.55 (s, 1H), 7.21–7.05 (m, 2H), 6.90 (dd, *J* = 6.3, 3.3 Hz, 1H), 5.22 (bs, 1H), 4.74 (s, 2H), 3.86–3.70 (m, 1H), 3.01 (bs, 4H), 2.89 (t, *J* = 7.4 Hz, 2H), 2.64 (bs, 4H), 2.55 (t, *J* = 6.7 Hz, 2H), 2.19–2.05 (m, 2H), 1.90–1.74 (m, 2H), 1.70–1.50 (m, 2H), 1.42–1.19 (m, 3H), 1.15–0.85 (m, 3H). ¹³C NMR (75 MHz, CDCl₃) δ (ppm): 164.8, 157.4, 151.2, 143.2, 135.3, 134.2, 127.6, 124.8, 124.2, 118.7, 118.3, 118.2, 113.8, 107.4, 57.3, 53.3, 51.3, 49.0, 47.1, 33.0, 25.3, 25.1, 24.8, 24.4. HRMS (CI) *m/z* calcd for C₂₈H₃₄Br₂Cl₂N₅O [*M* + *H*]⁺: 684.0507, found: 684.0494.

N-(*tert*-Butyl)-2-(5,6-dibromo-2-(3-(4-(2,3-dichlorophenyl)piperazin-1-yl)propyl)-1*H*-benzo[d]imidazol-1-yl)acetamide (**24f**). Yield: 47%. Mp: 160–163 °C. ¹H NMR (300 MHz, CDCl₃) δ (ppm): 8.00 (s, 1H), 7.54 (s, 1H), 7.18–7.10 (m, 2H), 6.90 (dd, *J* = 6.3, 3.3 Hz, 1H), 5.20 (bs, 1H), 4.66 (s, 2H), 3.01 (bs, 4H), 2.89 (t, *J* = 7.4 Hz, 2H), 2.64 (bs, 4H), 2.55 (t, *J* = 6.8 Hz, 2H), 2.19–2.05 (m, 2H), 1.30 (s, 9H). ¹³C NMR (75 MHz, CDCl₃) δ (ppm): 164.9, 157.4, 151.1, 142.8, 135.3, 134.1, 127.5, 124.8, 123.8, 123.7, 118.7, 117.9, 117.7, 113.6, 57.3, 53.2, 52.3, 51.1, 47.1, 28.7, 25.1, 24.2. HRMS (CI) *m/z* calcd for C₂₆H₃₂Br₂Cl₂N₅O [*M* + *H*]⁺: 658.0351, found: 658.0334.

General Procedure for the Synthesis of 4-(4-(4-(2,3-Dichlorophenyl)piperazin-1-yl)butanoyl)-3,4-dihydropyrazin-2(1*H*)-one Derivatives (26a–c). A mixture of 4-(4-(2,3-dichlorophenyl)piperazin-1-yl)butanoic acid **16** (0.47 mmol), formaldehyde **18a** (0.47 mmol), aminoacetaldehyde dimethyl acetal **17d** (0.47 mmol), and the corresponding isocyanide (**19a–c**) (0.63 mmol) in methanol (2 mL) was stirred at 25 °C for 48 h. The reaction was monitored by TLC. After completion of the reaction, PS-*p*-TsOH (2.0 mmol) and CH₂Cl₂ (3 mL) were added. The reaction mixture was submitted to orbital stirring at room temperature until complete consumption of the unreacted isocyanide (30–60 min). The polystyrene-supported salt was filtered off and successively washed with MeOH (3 × 5 mL) and CH₂Cl₂ (3 × 5 mL). To the polystyrene-supported salt was added CH₂Cl₂ (3 mL) and DIPEA (1.41 mmol), and the mixture was submitted to orbital stirring at

room temperature for 60 min. The polystyrene-supported salt was filtered off and successively washed with MeOH (3 × 5 mL) and CH₂Cl₂ (3 × 5 mL). The solutions were combined and evaporated to dryness. The residue was dissolved in a 50% solution of trifluoroacetic acid in dichloroethane, and the reaction mixture was stirred at 70 °C for 3 h. After the completion of the reaction, the mixture was neutralized with saturated aqueous NaHCO₃ and the product was extracted with AcOEt (2 × 10 mL) and CH₂Cl₂ (2 × 10 mL). The organic layers were combined and dried with Na₂SO₄, and the resulting oil was purified by column chromatography on silica gel using MeOH/CH₂Cl₂.

1-Benzyl-4-(4-(4-(2,3-dichlorophenyl)piperazin-1-yl)butanoyl)-3,4-dihydropyrazin-2(1*H*)-one (**26a**). Yield: 15%. Mp: 120–122 °C. ¹H NMR (300 MHz, CDCl₃) δ (ppm) (Mixture of rotamers): 7.37–7.17 (m, 5H), 7.16–7.04 (m, 2H), 6.90 (dd, *J* = 6.5, 3.2 Hz, 1H), 6.67 (d, *J* = 6.3 Hz, 0.3H), 6.20 (d, *J* = 6.1 Hz, 0.7H), 5.58 (d, *J* = 6.3 Hz, 0.3H), 5.53 (d, *J* = 6.1 Hz, 0.7H), 4.66 (s, 2H), 4.39 (s, 2H), 3.03 (bs, 4H), 2.69 (bs, 4H), 2.57–2.47 (m, 2H), 2.47–2.34 (m, 2H), 1.98–1.81 (m, 2H). ¹³C NMR (75 MHz, CDCl₃) δ (ppm): 170.3, 163.4, 150.8, 135.9, 133.9, 128.8, 128.0, 127.5, 127.4, 124.7, 118.7, 112.7, 109.4, 57.2, 52.9, 50.8, 48.7, 45.9, 30.5, 21.2. HRMS (CI) *m/z* calcd for C₂₅H₂₉Cl₂N₄O₂ [*M* + *H*]⁺: 487.1668, found: 487.1675.

1-Cyclohexyl-4-(4-(4-(2,3-dichlorophenyl)piperazin-1-yl)butanoyl)-3,4-dihydropyrazin-2(1*H*)-one (**26b**). Yield: 17%. Mp: 113–115 °C. ¹H NMR (300 MHz, CDCl₃) δ (ppm) (Mixture of rotamers): 7.19–7.05 (m, 2H), 6.93 (dd, *J* = 6.0, 3.6 Hz, 1H), 6.70 (d, *J* = 6.4 Hz, 0.3H), 6.24 (d, *J* = 6.2 Hz, 0.7H), 5.71 (d, *J* = 6.5 Hz, 0.3H), 5.65 (d, *J* = 6.2 Hz, 0.7H), 4.49–4.36 (m, 1H), 4.34 (s, 2H), 3.04 (bs, 4H), 2.62 (bs, 4H), 2.51–2.36 (m, 4H), 1.97–1.84 (m, 2H), 1.84–1.76 (m, 3H), 1.76–1.61 (m, 2H), 1.48–1.25 (m, 5H). ¹³C NMR (75 MHz, CDCl₃) δ (ppm): 170.3, 162.9, 151.0, 134.0, 127.4, 124.6, 118.6, 109.3, 109.1, 109.0, 57.3, 53.1, 51.7, 51.0, 46.1, 30.8, 30.7, 25.5, 25.3, 21.5. HRMS (CI) *m/z* calcd for C₂₄H₃₃Cl₂N₄O₂ [*M* + *H*]⁺: 479.1981, found: 479.1991.

1-(*tert*-Butyl)-4-(4-(4-(2,3-dichlorophenyl)piperazin-1-yl)butanoyl)-3,4-dihydropyrazin-2(1*H*)-one (**26c**). Yield: 15%. Mp: 139–141 °C. ¹H NMR (300 MHz, CDCl₃) δ (ppm) (Mixture of rotamers): 7.19–7.07 (m, 2H), 6.94 (dd, *J* = 6.0, 3.7 Hz, 1H), 6.58 (d, *J* = 6.5 Hz, 0.3H), 6.14 (d, *J* = 6.3 Hz, 0.7H), 5.94 (d, *J* = 6.6 Hz, 0.3H), 5.86 (d, *J* = 6.3 Hz, 0.7H), 4.26 (s, 2H), 3.04 (bs, 4H), 2.63 (bs, 4H), 2.53–2.34 (m, 4H), 2.01–1.81 (m, 2H), 1.47 (s, 9H). ¹³C NMR (75 MHz, CDCl₃) δ (ppm): 170.1, 164.3, 151.1, 134.0, 127.5, 127.4, 124.7, 118.6, 111.6, 108.6, 58.3, 57.4, 53.1, 51.1, 47.5, 30.6, 28.5, 21.5. HRMS (CI) *m/z* calcd for C₂₂H₃₁Cl₂N₄O₂ [*M* + *H*]⁺: 453.1824, found: 453.1805.

General Procedure for the Synthesis of 1-(4-(4-(2,3-Dichlorophenyl)piperazin-1-yl)butanoyl)-4-methylpiperazine-2-carboxamide Derivatives (27a–c). A mixture of 4-(4-(2,3-dichlorophenyl)piperazin-1-yl)butanoic acid **16** (0.63 mmol), 2-chloroacetaldehyde **18c** (0.63 mmol), N¹-methylpropane-1,3-diamine **17e** (0.63 mmol), the corresponding isocyanide (**19a–c**) (0.63 mmol), and NaHCO₃ (0.95 mmol) in trifluoroethanol (2 mL) was stirred at 25 °C for 72 h. The reaction was monitored by TLC. After completion of the reaction, PS-*p*-TsOH (2.0 mmol) and CH₂Cl₂ (3 mL) were added. The reaction mixture was submitted to orbital stirring at room temperature until complete consumption of the unreacted isocyanide (30–60 min). The polystyrene-supported salt was filtered off and successively washed with MeOH (3 × 5 mL) and CH₂Cl₂ (3 × 5 mL). Solvents were combined and evaporated to dryness. The resulting oil was purified by column chromatography on silica gel using MeOH/CH₂Cl₂.

(±) *N*-Benzyl-1-(4-(4-(2,3-dichlorophenyl)piperazin-1-yl)butanoyl)-4-methylpiperazine-2-carboxamide (**27a**). Yield: 10%. Mp: 66–68 °C. ¹H NMR (300 MHz, CDCl₃) δ (ppm) (Mixture of rotamers): 8.00 (bs, 0.5H), 7.44–7.19 (m, 5H), 7.19–7.06 (m, 2H),

7.00–6.85 (m, 1H), 6.57 (bs, 0.5H), 5.26–5.12 (m, 0.5H), 4.60–4.36 (m, 2.5H), 3.81–3.68 (m, 0.5H), 3.51–3.35 (m, 1H), 3.30–3.18 (m, 0.5H), 3.11–2.98 (m, 4H), 2.95–2.75 (m, 2H), 2.71–2.58 (m, 5H), 2.51–2.41 (m, 3H), 2.30 (s, 1.5H), 2.28 (s, 1.5H), 2.10–1.77 (m, 4H). ¹³C NMR (75 MHz, CDCl₃) δ (ppm): 172.8, 169.5, 138.1, 134.0, 128.9, 128.8, 128.7, 127.6, 127.5, 124.7, 124.6, 123.1, 118.6, 57.7, 55.6, 54.7, 54.4, 53.2, 51.2, 46.2, 43.5, 38.6, 30.8, 22.1. HRMS (CI) *m/z* calcd for C₂₇H₃₆Cl₂N₅O₂ [M + H]⁺: 532.2246, found: 532.2246.

(±) *N*-Cyclohexyl-1-(4-(4-(2,3-dichlorophenyl)piperazin-1-yl)butanoyl)-4-methylpiperazine-2-carboxamide (**27b**). Yield: 13%. Brown oil. ¹H NMR (300 MHz, CDCl₃) δ (ppm): 7.20–7.10 (m, 2H), 7.03–6.92 (m, 1H), 6.71 (bs, 1H), 4.43–4.25 (m, 1H), 3.81–3.70 (m, 1H), 3.49–3.30 (m, 1H), 3.27–3.02 (m, 5H), 2.85–2.48 (m, 8H), 2.30 (s, 3H), 2.08–1.77 (m, 6H), 1.48–1.04 (m, 10H). ¹³C NMR (75 MHz, CDCl₃) δ (ppm): 169.5, 168.2, 149.0, 134.1, 127.6, 118.9, 118.8, 96.7, 57.6, 55.7, 53.1, 52.8, 45.9, 43.8, 40.7, 33.1, 33.0, 32.9, 32.8, 29.7, 25.5, 25.5, 24.8, 24.5, 22.7, 14.1. HRMS (CI) *m/z* calcd for C₂₆H₄₀Cl₂N₅O₂ [M + H]⁺: 524.2559, found: 524.2560.

(±) *N*-(*tert*-Butyl)-1-(4-(4-(2,3-dichlorophenyl)piperazin-1-yl)butanoyl)-4-methylpiperazine-2-carboxamide (**27c**). Yield: 10%. Brown oil. ¹H NMR (300 MHz, CDCl₃) δ (ppm) (Mixture of rotamers): 7.79 (bs, 0.6H), 7.20–7.05 (m, 2H), 6.95 (dd, *J* = 6.4, 3.3 Hz, 1H), 6.15 (bs, 0.4H), 5.07–4.96 (m, 0.4H), 4.57–4.42 (m, 0.6H), 4.37–4.22 (m, 0.6H), 3.79–3.66 (m, 0.4H), 3.48–3.36 (m, 0.4H), 3.36–3.26 (m, 0.6H), 3.18–2.97 (m, 4H), 2.97–2.74 (m, 2H), 2.72–2.59 (m, 4H), 2.59–2.34 (m, 4H), 2.28 (s, 3H), 2.24–2.09 (m, 1H), 2.07–1.77 (m, 3H), 1.33 (s, 9H). ¹³C NMR (75 MHz, CDCl₃) δ (ppm): 172.8, 169.0, 168.7, 151.2, 134.1, 127.6, 124.8, 118.8, 57.8, 57.1, 55.8, 54.8, 54.6, 53.2, 53.0, 51.3, 51.0, 45.8, 38.4, 30.8, 29.0, 28.9, 28.8, 22.0. HRMS (CI) *m/z* calcd for C₂₄H₃₈Cl₂N₅O₂ [M + H]⁺: 498.2403, found: 498.2404.

General Procedure for the Synthesis of 1-(4-(4-(2,3-Dichlorophenyl)piperazin-1-yl)butanoyl)-3-oxopiperazine-2-carboxamide Derivatives (29a–c). A mixture of 4-(4-(2,3-dichlorophenyl)piperazin-1-yl)butanoic acid **16** (0.63 mmol), ethyl glyoxylate **18d** (0.63 mmol), *N*-BOC-ethylenediamine **17f** (0.63 mmol), and the corresponding isocyanide (**19a–c**) (0.63 mmol) in methanol (2 mL) was stirred at 25 °C for 48 h. The reaction was monitored by TLC. After completion of the reaction, PS-*p*-TsOH (2.0 mmol) and CH₂Cl₂ (3 mL) were added. The reaction mixture was submitted to orbital stirring at room temperature until complete consumption of the unreacted isocyanide (30–60 min). The polystyrene-supported salt was filtered off and successively washed with MeOH (3 × 5 mL) and CH₂Cl₂ (3 × 5 mL). To the polystyrene-supported salt was added CH₂Cl₂ (3 mL) and DIPEA (1.9 mmol), and the mixture was submitted to orbital stirring at room temperature for 60 min. The polystyrene-supported salt was filtered off and successively washed with MeOH (3 × 5 mL) and CH₂Cl₂ (3 × 5 mL). The solutions were combined and evaporated to dryness. The residue was dissolved in a 10% solution of trifluoroacetic acid in dichloroethane, and the reaction mixture was stirred at 25 °C for 12 h. After completion of the reaction, the mixture was neutralized with a saturated solution of NaHCO₃ and the product was extracted with AcOEt (2 × 10 mL) and CH₂Cl₂ (2 × 10 mL). The organic layers were combined and dried with Na₂SO₄, and the resulting oil was purified by column chromatography on silica gel using MeOH/CH₂Cl₂.

(±) *N*-Benzyl-1-(4-(4-(2,3-dichlorophenyl)piperazin-1-yl)butanoyl)-3-oxopiperazine-2-carboxamide (**29a**). Yield: 19%. Mp: 160–162 °C. ¹H NMR (300 MHz, CDCl₃) δ (ppm) (Mixture of rotamers): 7.82 (t, *J* = 5.5 Hz, 0.3H), 7.42 (t, *J* = 5.5 Hz, 0.7H), 7.34–7.18 (m, 5H), 7.17–7.05 (m, 2H), 6.94 (dd, *J* = 6.4, 3.1 Hz, 1H), 6.92–6.79 (m, 1H), 5.51 (s, 0.7H), 5.19 (s, 0.3H), 4.80–4.67 (m, 0.3H), 4.59–4.31 (m, 2H), 4.03–3.86 (m, 1H), 3.71–3.54 (m, 0.7H), 3.50–3.31 (m, 2H), 3.04 (bs, 4H), 2.63 (bs, 4H), 2.53–2.34 (m, 2H), 2.34–2.16 (m, 2H), 2.01–1.74 (m, 2H). ¹³C NMR (75 MHz, CDCl₃) δ (ppm): 172.1, 166.6, 164.8, 151.1, 137.8, 134.0, 128.7, 128.6, 127.6, 127.5, 124.6, 118.6, 61.4, 58.8, 57.4, 53.1, 51.0,

43.8, 41.1, 30.6, 21.7. HRMS (CI) *m/z* calcd for C₂₆H₃₂Cl₂N₅O₃ [M + H]⁺: 532.1882, found: 532.1887.

(±) *N*-Cyclohexyl-1-(4-(4-(2,3-dichlorophenyl)piperazin-1-yl)butanoyl)-3-oxopiperazine-2-carboxamide (**29b**). Yield: 11%. Mp: 92–94 °C. ¹H NMR (300 MHz, CDCl₃) δ (ppm) (Mixture of rotamers): 7.33 (d, *J* = 8.0 Hz, 0.6H), 7.19–7.06 (m, 2H), 6.93 (dt, *J* = 6.7, 3.5 Hz, 1H), 6.79 (d, *J* = 8.5 Hz, 0.4H), 6.68–6.48 (m, 1H), 5.46 (s, 0.6H), 5.08 (s, 0.4H), 4.80–4.65 (m, 0.4H), 4.03–3.91 (m, 0.6H), 3.81–3.54 (m, 2H), 3.53–3.22 (m, 2H), 3.05 (bs, 4H), 2.97–2.81 (m, 0.4H), 2.80–2.52 (m, 5H), 2.55–2.33 (m, 1.8H), 2.37–2.20 (m, 0.8H), 1.98–1.76 (m, 4H), 1.75–1.60 (m, 2H), 1.39–1.07 (m, 6H). ¹³C NMR (75 MHz, CDCl₃) δ (ppm): 172.0, 166.8, 163.4, 151.1, 134.0, 127.5, 127.4, 124.6, 118.6, 58.7, 57.4, 53.1, 51.1, 48.9, 41.3, 40.8, 32.8, 32.7, 30.6, 25.4, 24.7, 24.6, 21.8. HRMS (CI) *m/z* calcd for C₂₅H₃₆Cl₂N₅O₃ [M + H]⁺: 524.2195, found: 524.2189.

(±) *N*-(*tert*-Butyl)-1-(4-(4-(2,3-dichlorophenyl)piperazin-1-yl)butanoyl)-3-oxopiperazine-2-carboxamide (**29c**). Yield: 12%. Mp: 164–166 °C. ¹H NMR (300 MHz, CDCl₃) δ (ppm) (Mixture of rotamers): 7.28 (s, 0.4H), 7.19–7.07 (m, 2H), 6.95 (dd, *J* = 6.3, 3.3 Hz, 1H), 6.82 (s, 0.6H), 6.30 (s, 0.6H), 6.26 (s, 0.4H), 5.43 (s, 0.6H), 5.01 (s, 0.4H), 4.84–4.68 (m, 0.4H), 4.04–3.85 (m, 1H), 3.69–3.55 (m, 0.6H), 3.55–3.23 (m, 2H), 3.07 (bs, 4H), 2.96–2.78 (m, 0.4H), 2.66 (bs, 4H), 2.60–2.38 (m, 3H), 2.32–2.20 (m, 0.6H), 2.02–1.81 (m, 2H), 1.36 (s, 3H), 1.34 (s, 6H). ¹³C NMR (75 MHz, CDCl₃) δ (ppm): 171.9, 167.1, 163.2, 151.1, 134.0, 127.5, 127.4, 124.6, 118.6, 59.1, 57.5, 53.2, 53.1, 51.7, 51.1, 41.3, 40.7, 30.6, 28.6, 21.8. HRMS (CI) *m/z* calcd for C₂₃H₃₄Cl₂N₅O₃ [M + H]⁺: 498.2039, found: 498.2029.

Biological Evaluation. Cell Culture and Transient Transfection. HEK-293T cells were grown in Dulbecco's modified medium (DMEM) (Gibco, Paisley, Scotland, UK) supplemented with 2 mM L-glutamine, 100 U/mL penicillin/streptomycin, MEM non-essential amino acids solution (1/100), and 5% (v/v) heat-inactivated fetal bovine serum (FBS) (Invitrogen, Paisley, Scotland, UK). Cells were maintained in a humid atmosphere of 5% CO₂ at 37 °C. Cells were transiently transfected with the PEI (polyethylenimine, Sigma-Aldrich) method as previously described.⁵⁷

cAMP Determination. HEK-293T cells were transiently transfected with 0.5 μg of cDNA for DRD₂, DRD₃, or DRD₄ with the PEI method. Two hours before initiating the experiment, the cell medium was exchanged to the non-supplemented DMEM medium. The cells were then detached and suspended in the medium containing 50 μM zardaverine. Cells were placed in 384-well plates (2500 cells/well), pretreated with antagonists or vehicle (15 min) and stimulated with agonists (15 min) before adding 0.5 μM forskolin or vehicle (15 min). Readings were performed after 1 h of incubation at 25 °C. Homogeneous time-resolved fluorescence energy transfer (HTRF) measurements were carried out using the Lance Ultra cAMP kit (Perkin Elmer, Waltham, MA, USA). Fluorescence at 665 nm was analyzed on a PHERAstar Flagship plate reader equipped with an HTRF optical module (BMG Lab Technologies, Offenburg, Germany). The reference value (100%) was that achieved by 0.5 μM forskolin treatment. The effect of ligands is given as a percentage with respect to the reference value.

β-Arrestin 2 Recruitment. HEK-293T cells were transiently transfected with 0.5 μg of cDNA β-arrestin 2-RLuc and with 0.6 μg of cDNA for DRD₂-YFP, DRD₃-YFP, or DRD₄-YFP by the PEI method. Arrestin recruitment was determined as previously described.⁵⁷ Briefly, BRET experiments were performed in HEK-293T cells 48 h after transfection with the cDNAs corresponding to the D₂R-YFP and 1 μg of cDNA corresponding to β-arrestin 2-RLuc. Cells (20 μg of protein) were distributed in 96-well microplates (Corning 3600, white plates with white bottom) and were stimulated with the specific compounds for 10 min prior the addition of 5 μM coelenterazine H. Ten minutes after adding coelenterazine H, BRET between β-arrestin 2-RLuc and receptor-YFP was determined and quantified. The readings were collected using a Mithras LB-940 system (Berthold Technologies, Bad Wildbad, Germany), which allows the integration of the signals detected in the short-wavelength filter at 485 nm and the long-wavelength filter at 530 nm. To quantify

protein-RLuc expression, luminescence readings were also performed 10 min after adding 5 μ M coelenterazine H.

Data Analysis. The data in graphs are the mean \pm S.D. GraphPad Prism software version 5 (San Diego, CA, USA) was used for data fitting and statistical analysis. One-way ANOVA followed by a post-hoc Bonferroni test was used. Significant differences were considered when $p < 0.05$.

Molecular Modeling. The structure of hDRD₂ in complex with the antagonist risperidone (PDB code 6CM4) and the active structure of the same receptor with agonist bromocriptine (PDB code 6VMS) were retrieved from the Protein Data Bank and prepared for docking purposes with the Protein Preparation Wizard from Maestro.⁶⁸ This stage included addition of hydrogens, assignment of tautomeric states of His, Asn, and Gln sidechains, protonation state of ionizable residues considering physiological pH, as well as filling missing sidechains, replacing the fusion protein T4L with a hexapeptide based on the intracellular tips of TM5-TM6, and connecting these (as well as TM3-TM4) with Prime.⁶⁸ The ligands with measured hDRD₂ affinities (Table 1) were generated in their 3D conformation with Maestro from the corresponding smiles strings, and the database of ligands on the different protonation and tautomeric states generated with LigPrep. Three independent docking strategies were followed: (i) flexible ligand superposition within Maestro, using risperidone as a scaffold; (ii) automated docking with Glide, with the search box defined on the basis of the co-crystallized ligand (risperidone) and applying default single-precision (GlideSP) settings;⁶⁹ (iii) induced-fit docking on the active structure with the IFD protocol implemented in the Schrödinger suite,⁶⁸ with the search box defined on the basis of the co-crystallized ligand (bromocriptine). In each of these three strategies, one pose per ligand was retained, with separate stereo-isomeric species considered when there was a stereocenter.

■ ASSOCIATED CONTENT

Supporting Information

The Supporting Information is available free of charge at <https://pubs.acs.org/doi/10.1021/acs.jmedchem.1c00704>.

HPLC traces of lead compounds and HRMS (chemical ionization) of compounds **24d**, **24e**, and **24f** (PDF)
PDBs files (PDB, PDB)
Molecular formula strings (CSV)

■ AUTHOR INFORMATION

Corresponding Authors

Gemma Navarro – Department of Biochemistry and Physiology, Faculty of Pharmacy and Food Science, University of Barcelona, 08028 Barcelona, Spain; Centro de Investigación Biomédica en Red Enfermedades Neurodegenerativas (CIBERNED), 28031 Madrid, Spain; Phone: +34934021213; Email: g.navarro@ub.edu; Fax: +34934034500

Eddy Sotelo – Centro Singular de Investigación en Química Biológica e Materiais Moleculares (CIQUS) and Departamento de Química Orgánica, Facultade de Farmacia, Universidade de Santiago de Compostela, 15782 Santiago de Compostela, Spain; orcid.org/0000-0001-5571-2812; Phone: +34 881815732; Email: e.sotelo@usc.es; Fax: +34-881815704

Authors

Ana Mallo-Abreu – Centro Singular de Investigación en Química Biológica e Materiais Moleculares (CIQUS) and Departamento de Química Orgánica, Facultade de Farmacia, Universidade de Santiago de Compostela, 15782 Santiago de Compostela, Spain

Irene Reyes-Resina – Department of Biochemistry and Physiology, Faculty of Pharmacy and Food Science, University

of Barcelona, 08028 Barcelona, Spain; Centro de Investigación Biomédica en Red Enfermedades Neurodegenerativas (CIBERNED), 28031 Madrid, Spain
Jhony Azuaje – Centro Singular de Investigación en Química Biológica e Materiais Moleculares (CIQUS) and Departamento de Química Orgánica, Facultade de Farmacia, Universidade de Santiago de Compostela, 15782 Santiago de Compostela, Spain

Rafael Franco – Faculty of Chemistry, University of Barcelona, 08028 Barcelona, Spain; Centro de Investigación Biomédica en Red Enfermedades Neurodegenerativas (CIBERNED), 28031 Madrid, Spain; orcid.org/0000-0003-2549-4919

Aitor García-Rey – Centro Singular de Investigación en Química Biológica e Materiais Moleculares (CIQUS) and Departamento de Química Orgánica, Facultade de Farmacia, Universidade de Santiago de Compostela, 15782 Santiago de Compostela, Spain

Maria Majellaro – Centro Singular de Investigación en Química Biológica e Materiais Moleculares (CIQUS) and Departamento de Química Orgánica, Facultade de Farmacia, Universidade de Santiago de Compostela, 15782 Santiago de Compostela, Spain

Darío Miranda-Pastoriza – Centro Singular de Investigación en Química Biológica e Materiais Moleculares (CIQUS) and Departamento de Química Orgánica, Facultade de Farmacia, Universidade de Santiago de Compostela, 15782 Santiago de Compostela, Spain

Xerardo García-Mera – Departamento de Química Orgánica, Facultade de Farmacia, Universidade de Santiago de Compostela, 15782 Santiago de Compostela, Spain

Willem Jespers – Department of Cell and Molecular Biology, Uppsala University, Uppsala SE-75124, Sweden; orcid.org/0000-0002-4951-9220

Hugo Gutiérrez-de-Terán – Department of Cell and Molecular Biology, Uppsala University, Uppsala SE-75124, Sweden; orcid.org/0000-0003-0459-3491

Complete contact information is available at: <https://pubs.acs.org/doi/10.1021/acs.jmedchem.1c00704>

Notes

The authors declare no competing financial interest.

■ ACKNOWLEDGMENTS

This work was financially supported by the Consellería de Cultura, Educación e Ordenación Universitaria of the Galician Government: (grant: ED431B 2020/43), Centro Singular de Investigación de Galicia accreditation 2019-2022 (ED431G 2019/03), the Spanish Ministerio de Economía y Competitividad (SAF2017-84117-R), the European Regional Development Fund (ERDF) and the Swedish Research Council. Additional support from the Swedish strategic research program eSENCE and Deputación da Coruña (grant: 2019000011466) are acknowledged. The computations were performed on resources provided by the Swedish National Infrastructure for Computing (SNIC). This research program was developed within the framework of the European COST action ERNEST (CA 18133).

■ ABBREVIATIONS USED

7TMR, seven transmembrane receptors; APD, antipsychotic drug; DMEM, Dulbecco's modified medium; DR, dopamine receptors; DRD₂, dopamine D₂ receptor; DRD₃, dopamine D₃

receptor; DRD₄, dopamine D₃ receptor; EBD, extended binding domain; EPS, extrapyramidal symptoms; GPCR, G protein-coupled receptor; HEK-293T, human embryonic kidney cell; LHS, left-hand side; MCR, multicomponent reaction; MOR, μ -opioid receptor; MPLC, medium-pressure liquid chromatography; PEI, polyethyleneimine; PLS, parallel reaction synthesizer; PP, primary pharmacophore; RHS, right-hand side; SD, standard deviation; SFSR, structure–functional selectivity relationship; SP, secondary pharmacophore; U-4CR, Ugi four-component reaction; UDC, Ugi-Deprotection-Cyclization

REFERENCES

- (1) Lagerström, M. C.; Schiöth, H. B. Structural Diversity of G Protein-Coupled Receptors and Significance for Drug Discovery. *Nat. Rev. Drug Discov.* **2008**, *7*, 339–357.
- (2) Santos, R.; Ursu, O.; Gaulton, A.; Bento, A. P.; Donadi, R. S.; Bologa, C. G.; Karlsson, A.; Al-Lazikani, B.; Hersey, A.; Oprea, T. I.; Overington, J. P. A Comprehensive Map of Molecular Drug Targets. *Nat. Rev. Drug Discov.* **2017**, *16*, 19–34.
- (3) Smith, J. S.; Lefkowitz, R. J.; Rajagopal, S. Biased Signalling: From Simple Switches to Allosteric Microprocessors. *Nat. Rev. Drug Discov.* **2018**, *17*, 243–260.
- (4) Urban, J. D.; Clarke, W. P.; Von Zastrow, M.; Nichols, D. E.; Kobilka, B.; Weinstein, H.; Javitch, J. A.; Roth, B. L.; Christopoulos, A.; Sexton, P. M.; Miller, K. J.; Spedding, M.; Mailman, R. B. Functional Selectivity and Classical Concepts of Quantitative Pharmacology. *J. Pharmacol. Exp. Ther.* **2007**, *320*, 1–13.
- (5) Shenoy, S. K.; Lefkowitz, R. J. β -Arrestin-Mediated Receptor Trafficking and Signal Transduction. *Trends Pharmacol. Sci.* **2011**, *32*, 521–533.
- (6) Yun, Y.; Ji, J.; Lee, H. H. Dissecting the Structural Features of β -Arrestins as Multifunctional Proteins. *Biochim Biophys Acta Proteins Proteom.* **2021**, *1869*, 140603.
- (7) Kenakin, T. Biased Receptor Signaling in Drug Discovery. *Pharmacol. Rev.* **2019**, *71*, 267–315.
- (8) Shchepinova, M. M.; Hanyaloglu, A. C.; Frost, G. S.; Tate, E. W. Chemical Biology of Noncanonical G Protein–Coupled Receptor Signaling: Toward Advanced Therapeutics. *Curr. Opin. Chem. Biol.* **2020**, *56*, 98–110.
- (9) Seyedabadi, M.; Ghahremani, M. H.; Albert, P. R. Biased Signaling of G Protein Coupled Receptors (GPCRs): Molecular Determinants of GPCR/Transducer Selectivity and Therapeutic Potential. *Pharmacol. Ther.* **2019**, *200*, 148–178.
- (10) Brogi, S.; Tafi, A.; Désaubry, L.; Nebigil, C. G. Discovery of GPCR Ligands for Probing Signal Transduction Pathways. *Front. Pharmacol.* **2014**, *5*, 255.
- (11) Correll, C. C.; McKittrick, B. A. Biased Ligand Modulation of Seven Transmembrane Receptors (7TMRs): Functional Implications for Drug Discovery. *J. Med. Chem.* **2014**, *57*, 6887–6896.
- (12) Tan, L.; Yan, W.; McCorvy, J. D.; Cheng, J. Biased Ligands of G Protein-Coupled Receptors (GPCRs): Structure-Functional Selectivity Relationships (SFSRs) and Therapeutic Potential. *J. Med. Chem.* **2018**, *61*, 9841–9878.
- (13) Manglik, A.; Lin, H.; Aryal, D. K.; McCorvy, J. D.; Dengler, D.; Corder, G.; Levit, A.; Kling, R. C.; Bernat, V.; Hübner, H.; Huang, X.; Sassano, M. F.; Giguère, P. M.; Löber, S.; Duan, D.; Scherrer, G.; Kobilka, B. K.; Gmeiner, P.; Roth, B. L.; Shoichet, B. K. Structure-Based Discovery of Opioid Analgesics with Reduced Side Effects. *Nature* **2016**, *537*, 185–190.
- (14) Soergel, D. G.; Subach, R. A.; Burnham, N.; Lark, M. W.; James, I. E.; Sadler, B. M.; Skobieranda, F.; Violin, J. D.; Webster, L. R. Biased Agonism of the μ -Opioid Receptor by TRV130 Increases Analgesia and Reduces on-Target Adverse Effects versus Morphine: A Randomized, Double-Blind, Placebo-Controlled. Crossover Study in Healthy Volunteers. *Pain* **2014**, *155*, 1829–1835.
- (15) Che, T.; Dwivedi-Agnihotri, H.; Shukla, A. K.; Roth, B. L. Biased Ligands at Opioid Receptors: Current Status and Future Directions. *Sci. Signaling* **2021**, *14*, No. eaav0320.
- (16) Weichert, D.; Banerjee, A.; Hiller, C.; Kling, R. C.; Hübner, H.; Gmeiner, P. Molecular Determinants of Biased Agonism at the Dopamine D₂ Receptor. *J. Med. Chem.* **2015**, *58*, 2703–2717.
- (17) Bonifazi, A.; Yano, H.; Ellenberger, M. P.; Muller, L.; Kumar, V.; Zou, M. F.; Cai, N. S.; Guerrero, A. M.; Woods, A. S.; Shi, L.; Newman, A. H. Novel Bivalent Ligands Based on the Sumanitrolol Pharmacophore Reveal Dopamine D₂ Receptor (D₂R) Biased Agonism. *J. Med. Chem.* **2017**, *60*, 2890–2907.
- (18) Borroto-Escuela, D. O.; Wydra, K.; Filip, M.; Fuxe, K. A_{2A}R-D₂R Heteroreceptor Complexes in Cocaine Reward and Addiction. *Trends Pharmacol. Sci.* **2018**, *39*, 1008–1020.
- (19) Franco, R.; Reyes-Resina, I.; Navarro, G. Dopamine in Health and Disease: Much More Than a Neurotransmitter. *Biomedicine* **2021**, *9*, 109.
- (20) Kehne, J.; Andree, T.; Heinrich, J. D₂ Receptor Partial Agonists: Treatment of CNS Disorders of Dopamine Function. *Curr. Top. Med. Chem.* **2008**, *8*, 1068–1088.
- (21) Urs, N. M.; Peterson, S. M.; Caron, M. G. New Concepts in Dopamine D₂ Receptor Biased Signaling and Implications for Schizophrenia Therapy. *Biol. Psychiatry* **2017**, *81*, 78–85.
- (22) Frankel, J. S.; Schwartz, T. L. Brexpiprazole and Cariprazine: Distinguishing Two New Atypical Antipsychotics from the Original Dopamine Stabilizer Aripiprazole. *Ther. Adv. Psychopharmacol.* **2017**, *7*, 29–41.
- (23) Citrome, L. The ABC's of Dopamine Receptor Partial Agonists - Aripiprazole, Brexpiprazole and Cariprazine: The 15-Min Challenge to Sort These Agents Out. *Int. J. Clin. Pract.* **2015**, *69*, 1211–1220.
- (24) Newman, A. H.; Battiti, F. O.; Bonifazi, A. 2016 Philip S. Portoghesi Medicinal Chemistry Lectureship: Designing Bivalent or Bitopic Molecules for G-Protein Coupled Receptors. The Whole Is Greater Than the Sum of Its Parts. *J. Med. Chem.* **2020**, *63*, 1779–1797.
- (25) Li, P.; Snyder, G. L.; Vanover, K. E. Dopamine Targeting Drugs for the Treatment of Schizophrenia: Past, Present and Future. *Curr. Top. Med. Chem.* **2016**, *16*, 3385–3403.
- (26) Designed Research; J, J. J. A. A.; Chen, X. Discovery of β -Arrestin-Biased Dopamine D₂ Ligands for Probing Signal Transduction Pathways Essential for Antipsychotic Efficacy. *PNAS* **2011**, *108*, 18488–18493.
- (27) Szabo, M.; Klein Herenbrink, C.; Christopoulos, A.; Lane, J. R.; Capuano, B. Structure-Activity Relationships of Privileged Structures Lead to the Discovery of Novel Biased Ligands at the Dopamine D₂ Receptor. *J. Med. Chem.* **2014**, *57*, 4924–4939.
- (28) Chen, X.; Sassano, M. F.; Zheng, L.; Setola, V.; Chen, M.; Bai, X.; Frye, S. V.; Wetsel, W. C.; Roth, B. L.; Jin, J. Structure–Functional Selectivity Relationship Studies of β -Arrestin-Biased Dopamine D₂ Receptor Agonists. *J. Med. Chem.* **2012**, *55* (16), 7141–7153.
- (29) Möller, D.; Banerjee, A.; Uzuneser, T. C.; Skultety, M.; Huth, T.; Plouffe, B.; Hübner, H.; Alzheimer, C.; Friedland, K.; Müller, C. P.; Bouvier, M.; Gmeiner, P. Discovery of G Protein-Biased Dopaminergics with a Pyrazolo[1,5-*a*]Pyridine Substructure. *J. Med. Chem.* **2017**, *60*, 2908–2929.
- (30) Chen, X.; McCorvy, J. D.; Fischer, M. G.; Butler, K. V.; Shen, Y.; Roth, B. L.; Jin, J. Discovery of G Protein-Biased D₂ Dopamine Receptor Partial Agonists. *J. Med. Chem.* **2016**, *59*, 10601–10618.
- (31) McCorvy, J. D.; Butler, K. V.; Kelly, B.; Rechsteiner, K.; Karpik, J.; Betz, R. M.; Kormos, B. L.; Shoichet, B. K.; Dror, R. O.; Jin, J.; Roth, B. L. Structure-Inspired Design of β -Arrestin-Biased Ligands for Aminergic GPCRs. *Nat. Chem. Biol.* **2018**, *14*, 126–134.
- (32) Bonifazi, A.; Yano, H.; Guerrero, A. M.; Kumar, V.; Hoffman, A. F.; Lupica, C. R.; Shi, L.; Newman, A. H. Novel and Potent Dopamine D₂ Receptor Go-Protein Biased Agonists. *ACS Pharmacol. Transl. Sci.* **2019**, *2*, 52–65.
- (33) Shen, Y.; McCorvy, J. D.; Martini, M. L.; Rodriguiz, R. M.; Pogorelov, V. M.; Ward, K. M.; Wetsel, W. C.; Liu, J.; Roth, B. L.; Jin,

- J. D₂ Dopamine Receptor G Protein-Biased Partial Agonists Based on Cariprazine. *J. Med. Chem.* **2019**, *62*, 4755–4771.
- (34) Free, R. B.; Chun, L. S.; Moritz, A. E.; Miller, B. N.; Doyle, T. B.; Conroy, J. L.; Padron, A.; Meade, J. A.; Xiao, J.; Hu, X.; Dulcey, A. E.; Han, Y.; Duan, L.; Titus, S.; Bryant-Genevier, M.; Barnaeva, E.; Ferrer, M.; Javitch, J. A.; Beuming, T.; Shi, L.; Southall, N. T.; Marugan, J. J.; Sibley, D. R. Discovery and Characterization of a G Protein-Biased Agonist That Inhibits β -Arrestin Recruitment to the D₂ Dopamine Receptor. *Mol. Pharmacol.* **2014**, *86*, 96–105.
- (35) Chun, L. S.; Vekariya, R. H.; Free, R. B.; Li, Y.; Lin, D. T.; Su, P.; Liu, F.; Namkung, Y.; Laporte, S. A.; Moritz, A. E.; Aubé, J.; Frankowski, K. J.; Sibley, D. R. Structure-Activity Investigation of a G Protein-Biased Agonist Reveals Molecular Determinants for Biased Signaling of the D₂ Dopamine Receptor. *Front. Synaptic Neurosci.* **2018**, *10*, 2.
- (36) Männel, B.; Dengler, D.; Shonberg, J.; Hübner, H.; Möller, D.; Gmeiner, P. Hydroxy-Substituted Heteroaryl piperazines: Novel Scaffolds for β -Arrestin-Biased D₂R Agonists. *J. Med. Chem.* **2017**, *60*, 4693–4713.
- (37) Jacobson, M.; Childers, W.; Abou-Gharbia, M. Dopamine D₂ Partial Agonists – Discovery, Evolution, and Therapeutic Potential. In *Successful Drug Discovery*; Wiley, 2019; Chap. 4, 83–130.
- (38) Männel, B.; Hübner, H.; Möller, D.; Gmeiner, P. β -Arrestin Biased Dopamine D₂ Receptor Partial Agonists: Synthesis and Pharmacological Evaluation. *Bioorganic Med. Chem.* **2017**, *25*, S613–S628.
- (39) Trincavelli, M. L.; Daniele, S.; Orlandini, E.; Navarro, G.; Casadó, V.; Giacomelli, C.; Nencetti, S.; Nuti, E.; Macchia, M.; Huebner, H.; Gmeiner, P.; Rossello, A.; Lluís, C.; Martini, C. A New D₂ Dopamine Receptor Agonist Allosterically Modulates A_{2A} Adenosine Receptor Signalling by Interacting with the A_{2A}/D₂ Receptor Heteromer. *Cell. Signal.* **2012**, *24*, 951–960.
- (40) Moritz, A. E.; Benjamin Free, R.; Sibley, D. R. Advances and Challenges in the Search for D₂ and D₃ Dopamine Receptor-Selective Compounds. *Cell. Signal.* **2018**, *41*, 75–81.
- (41) Roth, B. L.; Sheffer, D. J.; Kroeze, W. K. Magic Shotguns versus Magic Bullets: Selectively Non-Selective Drugs for Mood Disorders and Schizophrenia. *Nat. Rev. Drug Discov.* **2004**, *3*, 353–359.
- (42) Sexton, P. M.; Christopoulos, A. To Bind or Not to Bind: Unravelling GPCR Polypharmacology. *Cell* **2018**, *172*, 636–638.
- (43) Kopinathan, A.; Draper-Joyce, C.; Szabo, M.; Christopoulos, A.; Scammells, P. J.; Lane, J. R.; Capuano, B. Subtle Modifications to the Indole-2-Carboxamide Motif of the Negative Allosteric Modulator N-((trans)-4-(2-(7-cyano-3,4-dihydroisoquinolin-2(1H)-yl)ethyl)-cyclohexyl)-1H-indole-2-carboxamide (SB269652) Yield Dramatic Changes in Pharmacological Activity at the Dopamine D₂ Receptor. *J. Med. Chem.* **2019**, *62*, 371–377.
- (44) Löber, S.; Hübner, H.; Tschammer, N.; Gmeiner, P. Recent Advances in the Search for D₃- and D₄- Selective Drugs: Probes. *Models Candidates. Trends Pharmacol. Sci.* **2011**, *32*, 148–157.
- (45) Klein Herenbrink, C.; Verma, R.; Lim, H. D.; Kopinathan, A.; Keen, A.; Shonberg, J.; Draper-Joyce, C. J.; Scammells, P. J.; Christopoulos, A.; Javitch, J. A.; Capuano, B.; Shi, L.; Lane, R. Molecular Determinants of the Intrinsic Efficacy of the Antipsychotic Aripiprazole. *ACS Chem. Biol.* **2019**, *14*, 1780–1792.
- (46) Dömling, A.; Ugi, I. Multicomponent Reactions with Isocyanides. *Angew. Chemie* **2000**, *39*, 3168–3210.
- (47) Dömling, A.; Wang, W.; Wang, K. Chemistry and Biology Of Multicomponent Reactions. *Chem. Rev.* **2012**, *112*, 3083–3135.
- (48) Cioc, R. C.; Ruijter, E.; Orru, R. V. A. Multicomponent Reactions: Advanced Tools for Sustainable Organic Synthesis. *Green Chem.* **2014**, *16*, 2958–2975.
- (49) Abdelraheem, E. M. M.; Khaksar, S.; Kurpiewska, K.; Kalinowska-Tłuścik, J.; Shaabani, S.; Dömling, A. Two-Step Macrocycle Synthesis by Classical Ugi Reaction. *J. Org. Chem.* **2018**, *83*, 1441–1447.
- (50) Kurhade, S.; Diekstra, E.; Sutanto, F.; Kurpiewska, K.; Kalinowska-Tłuścik, J.; Dömling, A. Multicomponent Reaction Based Synthesis of 1-tetrazolyimidazo[1,5- a]pyridines. *Org. Lett.* **2018**, *20*, 3871–3874.
- (51) Madhavachary, R.; Zarganes-Tzitzikas, T.; Patil, P.; Kurpiewska, K.; Kalinowska-Tłuścik, J.; Dömling, A. Synthesis of Highly Substituted Imidazole Uracil Containing Molecules via Ugi-4CR and Passerini-3CR. *ACS Comb. Sci.* **2018**, *20*, 192–196.
- (52) Hulme, C.; Chappeta, S.; Griffith, C.; Lee, Y. S.; Dietrich, J. An Efficient Solution Phase Synthesis of Triazadibenzoazulenones: 'designer Isonitrile Free' Methodology Enabled by Microwaves. *Tetrahedron Lett.* **2009**, *50*, 1939–1942.
- (53) La Venia, A.; Lemrová, B.; Krchňák, V. Regioselective Incorporation of Backbone Constraints Compatible with Traditional Solid-Phase Peptide Synthesis. *ACS Comb. Sci.* **2013**, *15*, 59–72.
- (54) Rossen, K.; Sager, J.; Dimichele, L. M. An Efficient and Versatile Synthesis of Piperazine-2-Carboxamides. *Tetrahedron Lett.* **1997**, *38*, 3183–3186.
- (55) Hulme, C.; Cherrier, M. P. Novel Applications of Ethyl Glyoxalate with the Ugi MCR. *Tetrahedron Lett.* **1999**, *40*, S295–S299.
- (56) Reyes-Resina, I.; Samadi, A.; Navarro, G.; Saadeh, H. A.; Khasawneh, M. A.; Mestres, J.; Marco-Contelles, J.; Franco, R. Identification of a Tool Compound to Study the Mechanisms of Functional Selectivity between D₂ and D₃ Dopamine Receptors. *ACS Omega* **2018**, *3*, 17368–17375.
- (57) Navarro, G.; Cordero, A.; Brugarolas, M.; Moreno, E.; Aguinaga, D.; Pérez-Benito, L.; Ferre, S.; Cortés, A.; Casadó, V.; Mallol, J.; Canela, E. I.; Lluís, C.; Pardo, L.; McCormick, P. J.; Franco, R. Cross-Communication between Gi and Gs in a G-Protein-Coupled Receptor Heterotrimer Guided by a Receptor C-Terminal Domain. *BMC Biol.* **2018**, *16*, 24.
- (58) Tsuruta, K.; Frey, E. A.; Grewe, C. W.; Cote, T. E.; Eskay, R. L.; Keabian, J. W. Evidence That LY-141865 Specifically Stimulates the D-2 Dopamine Receptor. *Nature* **1981**, *292*, 463–465.
- (59) Van Der Westhuizen, E. T.; Breton, B.; Christopoulos, A.; Bouvier, M. Quantification of Ligand Bias for Clinically Relevant β_2 -Adrenergic Receptor Ligands: Implications for Drug Taxonomy S. *Mol. Pharmacol.* **2014**, *85*, 492–509.
- (60) Wang, S.; Che, T.; Levit, a.; Shoichet, B. K.; Wacker, D.; Roth, B. L. Structure of the D₂ Dopamine Receptor Bound to the Atypical Antipsychotic Drug Risperidone. *Nat. Publ. Gr.* **2018**, 269–273.
- (61) Wacker, D.; Fenalti, G.; Brown, M. A.; Katritch, V.; Abagyan, R.; Cherezov, V.; Stevens, R. C. Conserved Binding Mode of Human β_2 Adrenergic Receptor Inverse Agonists and Antagonist Revealed by X-Ray Crystallography. *J. Am. Chem. Soc.* **2010**, *132*, 11443–11445.
- (62) Zhou, Y.; Cao, C.; He, L.; Wang, X.; Zhang, X. C. Crystal Structure of Dopamine Receptor D₄ Bound to the Subtype Selective Ligand, L745870. *eLife* **2019**, *8*, e48822.
- (63) Chien, E. Y. T.; Liu, W.; Zhao, Q.; Katritch, V.; Han, G. W.; Hanson, M. A.; Shi, L.; Newman, A. H.; Javitch, J. A.; Cherezov, V.; Stevens, R. C. Structure of the Human Dopamine D₃ Receptor in Complex with a D₂/D₃ Selective Antagonist. *Science* **2010**, *330*, 1091–1095.
- (64) Fan, L.; Tan, L.; Chen, Z.; Qi, J.; Nie, F.; Luo, Z.; Cheng, J.; Wang, S. Haloperidol Bound D₂ Dopamine Receptor Structure Inspired the Discovery of Subtype Selective Ligands. *Nat. Commun.* **2020**, *11* ().
- (65) Yin, J.; Chen, K. Y. M.; Clark, M. J.; Hijazi, M.; Kumari, P.; Bai, X.; chen, Sunahara, R. K.; Barth, P.; Rosenbaum, D. M. Structure of a D₂ Dopamine Receptor–G-Protein Complex in a Lipid Membrane. *Nature* **2020**, *584*, 125–129.
- (66) Sherman, W.; Day, T.; Jacobson, M. P.; Friesner, R. A.; Farid, R. Novel Procedure for Modeling Ligand/Receptor Induced Fit Effects. *J. Med. Chem.* **2006**, *49*, 534–553.
- (67) Navarro, G.; Hradsky, J.; Lluís, C.; Casadó, V.; McCormick, P. J.; Kreutz, M. R.; Mikhaylova, M. NCS-1 Associates with Adenosine A_{2A} Receptors and Modulates Receptor Function. *Front. Mol. Neurosci.* **2012**, *5*, 53.
- (68) Schrödinger. *Schrödinger*. LLC New York 2009.

(69) Halgren, T. A.; Murphy, R. B.; Friesner, R. A.; Beard, H. S.; Frye, L. L.; Thomas Pollard, W.; Banks, J. L. Glide: A New Approach for Rapid, Accurate Docking and Scoring. 2. Enrichment Factors in Database Screening. *J. Med. Chem.* **2004**, *47*, 1750–1759.